Sensor-based globally exponentially stable range-only simultaneous localization and mapping

Pedro Lourenço, Pedro Batista, Paulo Oliveira, Carlos Silvestre,
and C.L. Philip Chen

Robotics and Autonomous Systems, vol. 68, pp. 72-85, June 2015

https://doi.org/10.1016/j.robot.2015.01.010

Accepted Version

Level of access, as per info available on SHERPA/ROMEO
http://www.sherpa.ac.uk/romeo/search.php

Robotics and Autonomous Systems

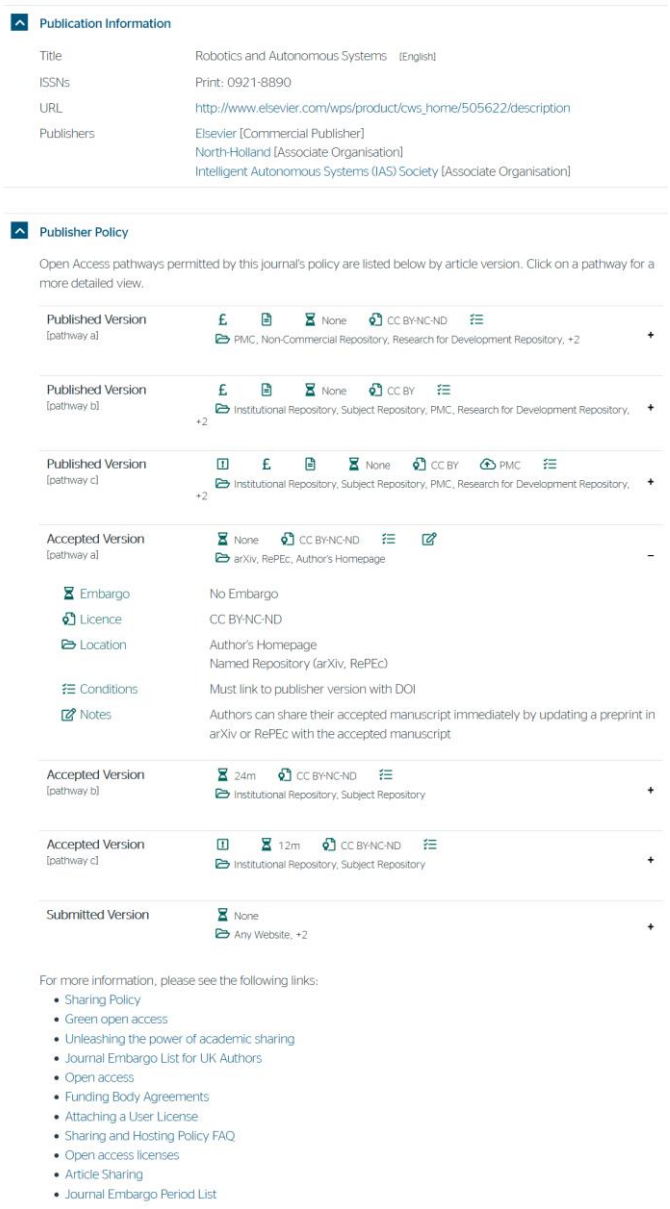

Sensor-based Globally Exponentially Stable Range-Only Simultaneous Localization and Mapping

Pedro Lourenço[a,*], Pedro Batista[a], Paulo Oliveira[a,b], Carlos Silvestre[a,c], C. L. Philip Chen[d]

[a] *Institute for Systems and Robotics, Instituto Superior Técnico, Universidade de Lisboa, Av. Rovisco Pais, 1049-001 Lisboa, Portugal*
[b] *Department of Mechanical Engineering, Instituto Superior Técnico, Universidade de Lisboa, Av. Rovisco Pais, 1049-001 Lisboa, Portugal*
[c] *Department of Electrical and Computer Engineering, Faculty of Science and Technology, University of Macau*
[d] *Department of Computer and Information Engineering, Faculty of Science and Technology, University of Macau*

Abstract

This paper proposes the design, analysis, and validation of a globally exponentially stable (GES) filter for tridimensional (3-D) range-only simultaneous localization and mapping. For observability analysis purposes, a nonlinear sensor-based dynamical system is formulated resorting only to exact linear and angular kinematics and a state augmentation is exploited that allows the proposed formulation to be considered as linear time-varying without linearizing the original nonlinear system. Constructive observability results can then be established, leading naturally to the design of a Kalman Filter with GES error dynamics. These results also provide valuable insight on the motion planning of the vehicle. Experimental results demonstrate the good performance of the algorithm and help validate the theoretical results presented. For completeness and to illustrate the necessity of a proper trajectory, simulation data are included as well.

Keywords: Simultaneous localization and mapping, Robot navigation, Autonomous vehicles, Nonlinear systems, Range data

1. Introduction

Simultaneous Localization and Mapping (SLAM) is the problem of navigating a vehicle in an unknown environment, by building a map of the area and using this map to deduce its location, without the need for a priori knowledge of

*Corresponding author
Email addresses: plourenco@isr.ist.utl.pt (Pedro Lourenço), pbatista@isr.ist.utl.pt (Pedro Batista), pjcro@isr.ist.utl.pt (Paulo Oliveira), cjs@isr.ist.utl.pt (Carlos Silvestre), philipchen@umac.mo (C. L. Philip Chen)

location. The solution to this problem is of great importance to the field of autonomous robots operating in GPS-denied environments, and therefore SLAM has been subject of intensive research by the community since first proposed in the 1980's, when a series of seminal works such as [1], [2], and [3] were published. From that initial discussion, a myriad of approaches have arisen. The better known include EKF-SLAM [4], graph-based solutions [5], and particle filters (see [6] and [7] for a two-part survey on all these algorithms). Apart from varying in concept, SLAM approaches also depend on different mapping sensors: SONAR [8], LIDAR [9], monocular and stereo cameras [10] are within the most common. These sensors involve obtaining range and bearing information of the environment, and usually demand the existence of a data association algorithm, due to the unknown correspondence between the reality and the created map.

Although localization using distances to beacons is a very well known subject, the number of SLAM algorithms using only ranges is relatively small, especially when compared with the widespread use of algorithms working on range and bearing, or on bearings-only. On one hand, the Range Only SLAM (RO-SLAM) problem is not prone to association errors, as are other SLAM formulations. In fact, this is a very relevant topic in this area, as can be seen by the variety of strategies proposed by the scientific community to minimize spurious associations, from general purpose algorithms such as the joint compatibility branch and bound [11] or more evolved strategies that make use of the unique characteristics of the detected features as the one proposed in [12]. RO-SLAM bypasses this error source due to the nature of the ranging signals that are usually tagged. Another of the issues in SLAM with both bearing and range information available that is avoided by RO-SLAM is the loop closing [13]. This is the problem of recognizing that a previously visited area is once again within the field-of-view of the vehicle. It is closely related to the association problem and with the inconsistency that some SLAM approaches suffer from, see [14]. In RO-SLAM, this is also not an issue, as the information carried by the ranging signals allows the unambiguous association of the measurement and the corresponding state at all times. On the other hand, one of the main problems in RO-SLAM is the initialization of the algorithm, either due to the absence of global convergence results in EKF solutions such as [15], or the computational burden of having a sufficiently representative prior belief, in particle filter solutions [16]. Most of the RO-SLAM solutions include some form of initializing procedure before inserting a new landmark in the state. These include trilateration with ranges from different instants to obtain a first estimate, usually through least squares, such as what was proposed in [17]. Also, due to the sparse information extracted from ranging, RO-SLAM algorithms are commonly designed for 2-D environments, e.g., a ground robot and landmarks at the same height, see [18].

The common RO-SLAM formulation has similarities with the problem of Sensor Networks (SN), in the sense that there is an agent receiving signals from a network of sensors, and, therefore, the two ideas have been used in conjunction in works such as [19] and [20], where, along with agent-to-sensor ranges, sensor-to-sensor ranges are also used.

This paper introduces a novel RO-SLAM algorithm that eliminates the landmark initialization problem through the establishment of global convergence results with a tridimensional (3-D) sensor-based formulation that avoids the representation of the pose of the vehicle in the state, as it becomes deterministic and available by construction. Furthermore, the sensor-based approach allows the direct use of odometry-like information that is usually expressed in body-fixed coordinates. This is related with previous results in the SLAM literature, such as the robocentric map joining [21] in which the filtering process is centered on the vehicle, while using an EKF to maintain estimates of both the map and the inertial vehicle pose. Another related work is Linear SLAM [22], in which the map joining procedure is followed, while the state is transformed and augmented in order to achieve a linear least squares formulation. The algorithm proposed in this paper relates to these works in the sense that the filter is designed in a body-fixed frame, while disposing of the vehicle pose. This solution is influenced by the source-localization algorithm proposed in [23], as the global convergence results are achieved through a similar state augmentation.

The main contributions of this paper are the design, analysis, and experimental validation of a 3-D RO-SLAM algorithm that (i) has globally exponentially stable (GES) error dynamics; (ii) resorts to the exact linear and angular motion kinematics; (iii) uses as odometry-like measurements the linear and angular velocities; (iv) solves a nonlinear problem with no linearizations whatsoever; and (v) builds on the well-established linear time-varying Kalman filtering theory. Note that, although the maps provided by this filter are body-fixed, it is possible to obtain an inertial estimate of both the map and the vehicle pose using, for example, the algorithm proposed in [24], in which a methodology was presented to obtain inertial estimates of the pose of the vehicle and of the landmark map using only the sensor-based map. This algorithm was successfully used with other purely sensor-based SLAM filters such as [25] and [26].

The constructive observability and convergence results achieved provide physical insight on what kind of trajectories the vehicle must take in order for the RO-SLAM algorithm to be able to perform accurately. These results were validated in real conditions, using a Cricket [27] sensor network as landmarks and an optical flow procedure to determine the linear velocity. Furthermore, simulation results are also presented to illustrate the good vertical performance when the trajectory is sufficiently rich, which was not possible to perform in the experiments carried out.

This problem was previously addressed by the authors in a preliminary version in [28]. This paper introduces new results on the observability of the designed nonlinear system, with the establishment of necessary conditions for observability, stability, and convergence that are important for trajectory planning. Furthermore, expanded and revised proofs for the theoretical results are presented, and more and better documented experiments are now reported.

The paper is organized as follows: in Section 2, the problem addressed in this paper is stated and the dynamics of the system to be filtered are presented; the observability analysis of the system is performed in Section 3 and filter implementation issues are detailed in Section 4. The results of simulation and

real experiments are presented in Sections 5 and 6, respectively, and, finally, Section 7 addresses some concluding remarks.

Notation. The superscript ^{I} indicates a vector or matrix expressed in the inertial frame $\{I\}$. For the sake of clarity, when no superscript is present, the vector is expressed in the body-fixed frame $\{B\}$. $\mathbf{I}_n$ is the identity matrix of dimension n, and $\mathbf{0}_{n\times m}$ is a n by m matrix filled with zeros. If m is omitted, the matrix is square. $\mathbf{S}[\mathbf{a}]$ is a special skew-symmetric matrix, henceforth called the cross-product matrix, as $\mathbf{S}[\mathbf{a}]\mathbf{b} = \mathbf{a} \times \mathbf{b}$ with $\mathbf{a}, \mathbf{b} \in \mathbb{R}^3$.

2. Problem statement and System dynamics

Consider a vehicle moving in a static world where acoustic beacons are installed at unknown locations. The vehicle is equipped with a sensor suite capable of measuring the linear and angular velocities as well as radio and acoustic signals from the static beacons. The distances to the emmitting beacons can then be computed from the time differences of arrival. This section details the design of a dynamical system as part of a simultaneous localization and mapping filter using only, apart from vehicle motion information, the distance to the beacons placed in the environment.

2.1. Problem statement

Assume the existence of two frames: a reference inertial frame $\{I\}$ and a body-fixed frame $\{B\}$. Points in the latter frame are mapped to the former through a rotation, given by the rotation matrix $\mathbf{R}(t) \in \mathrm{SO}(3)$ and a translation, given by ${}^I\mathbf{p}(t) \in \mathbb{R}^3$ that represent, respectively, the attitude and position of the vehicle. The rotation matrix respects the relation $\dot{\mathbf{R}}(t) = \mathbf{R}(t)\mathbf{S}\left[\boldsymbol{\omega}(t)\right]$, where $\boldsymbol{\omega}(t) \in \mathbb{R}^3$ is the angular velocity of the vehicle expressed in the body-fixed frame.

Let $\mathcal{L} := \{1, \ldots, N\}$ be a set of N landmarks fixed in the environment, to be mapped, containing, in each instant, N_O observed, or visible, landmarks in the set $\mathcal{L}_O$, and N_U unobserved, or invisible, landmarks in the set $\mathcal{L}_U$, such that $\mathcal{L} = \mathcal{L}_O \cup \mathcal{L}_U$. Furthermore, suppose that $\mathbf{p}_i(t) \in \mathbb{R}^3$ corresponds to a sensor-based landmark in the set $\mathcal{L}$, i.e., the position of the i-th landmark relative to the vehicle expressed in $\{B\}$, given by $\mathbf{p}_i(t) = \mathbf{R}^T(t)\left({}^I\mathbf{p}_i(t) - {}^I\mathbf{p}(t)\right)$, where ${}^I\mathbf{p}_i(t) \in \mathbb{R}^3$ corresponds to the inertial position of the landmark. Hence, the dynamics of any landmark expressed in the robotic vehicle coordinate system $\{B\}$ are given by

$$\dot{\mathbf{p}}_i(t) = -\mathbf{S}\left[\boldsymbol{\omega}(t)\right]\mathbf{p}_i(t) - \mathbf{v}(t),$$

where $\mathbf{v}(t) = \mathbf{R}^T(t){}^I\dot{\mathbf{p}}(t) \in \mathbb{R}^3$ is the linear velocity of the vehicle in $\{B\}$. Both the linear and angular velocities are available through sensor measurements. The distances to landmarks, henceforth denominated ranges, are given by $r_i(t) = \|{}^I\mathbf{p}_i(t) - {}^I\mathbf{p}(t)\| = \|\mathbf{p}_i(t)\|$ and are measured as well. Given that the landmarks positions are unknown a priori, the ranges are not sufficient to obtain

estimates of the coordinates of the landmarks, raising the need for the knowledge of the motion of the vehicle. That is why the linear velocity is measured.

This information motivates the design of a system whose states are the sensor-based landmarks and the linear velocity, and with outputs that are the ranges to the landmarks and the linear velocity. This system can be expressed through

$$\begin{cases} \dot{\mathbf{p}}_i(t) = -\mathbf{S}\left[\boldsymbol{\omega}(t)\right]\mathbf{p}_i(t) - \mathbf{v}(t) \\ \dot{\mathbf{v}}(t) = \mathbf{0} \\ r_i(t) = \|\mathbf{p}_i(t)\| \\ \mathbf{y}_v(t) = \mathbf{v}(t) \end{cases} \tag{1}$$

with $i \in \mathcal{L}$, and where the first two quantities are the system state and the last two its output. Although the linear velocity in $\{B\}$ is measured, it is included as a state with zero derivative for filtering purposes. Albeit being assumed constant in this deterministic setting, in the filtering framework it can be seen as slowly time-varying, depending on the process and measurement noise covariances.

The problem addressed in this paper is that of designing a navigation system for a vehicle operating in the environment previously described, by means of a filter for the dynamics in (1), assuming noisy measurements. The algorithm consists of a RO-SLAM filter in the space of sensors and, therefore, the pose of the vehicle is deterministic as it simply corresponds to the position and attitude of the body-fixed frame expressed in the same frame.

2.2. Augmented system dynamics

The system derived in the previous subsection is clearly nonlinear, as there is a nonlinear relation between the output and the system state. The strategy proposed to avoid this nonlinearity is to augment the system state in order to obtain a linear relation between the system state and output, as it has been successfully done in [23]. The resulting augmented state is

$$\mathbf{x}(t) := \begin{bmatrix} \mathbf{x}_L^T(t) & \mathbf{x}_V^T(t) & \mathbf{x}_R^T(t) \end{bmatrix}^T,$$

where $\mathbf{x}_L(t) \in \mathbb{R}^{n_L}$ is the vector built by stacking all the landmarks present in the landmark set $\mathcal{L}$, both the visible ones, $\mathbf{x}_{L_O}(t) := \{\mathbf{x}_{L_i}(t),\ i \in \mathcal{L}_O\}$, and the invisible ones, $\mathbf{x}_{L_U}(t) := \{\mathbf{x}_{L_i}(t),\ i \in \mathcal{L}_U\}$, $\mathbf{x}_V(t) \in \mathbb{R}^{n_V}$ represents the vehicle state, i.e., the linear velocity of the vehicle in the body-fixed frame, and the vector $\mathbf{x}_R(t) := \begin{bmatrix} \mathbf{x}_{R_O}^T(t) & \mathbf{x}_{R_U}^T(t) \end{bmatrix}^T \in \mathbb{R}^{n_R}$ contains the ranges to all the landmarks in the visible and invisible sets. The following expression summarizes the relations that define the augmented state,

$$\begin{cases} \mathbf{x}_{L_i}(t) := \mathbf{p}_i(t) \\ \mathbf{x}_V(t) := \mathbf{v}(t) \\ x_{R_i}(t) := \|\mathbf{x}_{L_i}(t)\| \end{cases}, \tag{2}$$

where $\mathbf{x}_{L_i}(t) \in \mathbb{R}^3$ and $x_{R_i}(t) \in \mathbb{R}$ are part of the full landmark and full range states, respectively, for all $i \in \mathcal{L}$. It is important to notice that, both in the

landmark and range states, the first N_O quantities are the visible ones, while the $i \in \{N_O + 1, \ldots, N_U\}$ are the remaining. The state is chosen this way to simplify the forthcoming analysis, without loss of generality.

The dynamics of the landmark and vehicle states have already been defined in (1), hence, the derivative of the range, given by

$$\dot{r}_i(t) = -\frac{1}{r_i(t)} \mathbf{v}^T(t) \mathbf{p}_i(t), \tag{3}$$

is needed to derive the full dynamics. Note that, although the system output is now linear, the introduction of the ranges as states has created another nonlinearity to the dynamics. On the other hand, the velocity is directly available as a measurement, as is the distance $r_i(t)$ if the corresponding landmark is visible, i.e., if $i \in \mathcal{L}_O$. Therefore, it is possible to replace the dependence on the state for one on the system output. Observing that the output is given by

$$\mathbf{y}(t) = \begin{bmatrix} \mathbf{y}_v^T(t) & y_{R_1}(t) & \cdots & y_{R_{N_O}}(t) \end{bmatrix}^T,$$

where $\mathbf{y}_v(t) := \mathbf{v}(t)$ and $y_{R_i}(t) = r_i(t)$ for every $i \in \mathcal{L}_O$, it is possible to derive the dynamics of the augmented system, which are given by

$$\begin{cases} \dot{\mathbf{x}}(t) = \mathbf{A}_F(\mathbf{x}_{R_U}(t), \mathbf{y}(t), t)\mathbf{x}(t) \\ \mathbf{y}(t) = \mathbf{C}_F \mathbf{x}(t) \end{cases} \tag{4}$$

where

$$\mathbf{A}_F(\mathbf{x}_{R_U}(t), \mathbf{y}(t), t) = \begin{bmatrix} \mathbf{A}_L(t) & \mathbf{A}_{LV} & \mathbf{0}_{n_L \times n_R} \\ \mathbf{0}_{n_V \times n_L} & \mathbf{0}_{n_V} & \mathbf{0}_{n_V \times n_R} \\ \mathbf{A}_{RL}(\mathbf{x}_{R_U}(t), \mathbf{y}(t), t) & \mathbf{0}_{n_R \times n_V} & \mathbf{0}_{n_R} \end{bmatrix},$$

and

$$\mathbf{C}_F = \begin{bmatrix} \mathbf{0}_{3 \times n_L} & \mathbf{I}_3 & \mathbf{0}_{3 \times N_O} & \mathbf{0}_{3 \times N_U} \\ \mathbf{0}_{N_O \times n_L} & \mathbf{0}_{N_O \times 3} & \mathbf{I}_{N_O} & \mathbf{0}_{N_O \times N_U} \end{bmatrix}.$$

The dynamics matrix is composed by three block matrices, namely one that relates the landmark state to itself, given by

$$\mathbf{A}_L(t) := \operatorname{diag}\left(-\mathbf{S}\left[\boldsymbol{\omega}(t)\right], \ldots, -\mathbf{S}\left[\boldsymbol{\omega}(t)\right]\right),$$

another that relates the landmark and vehicle states,

$$\mathbf{A}_{LV} := \begin{bmatrix} -\mathbf{I}_3 & \cdots & -\mathbf{I}_3 \end{bmatrix}^T,$$

and finally the relation between landmark and range states,

$$\mathbf{A}_{RL}(\mathbf{x}_R(t), \mathbf{y}(t), t) := -\operatorname{diag}\left(\frac{\mathbf{y}_v^T(t)}{y_{R_1}(t)}, \ldots, \frac{\mathbf{y}_v^T(t)}{y_{R_{N_O}}(t)}, \frac{\mathbf{y}_v^T(t)}{x_{R_{N_O+1}}(t)}, \cdots, \frac{\mathbf{y}_v^T(t)}{x_{R_N}(t)}\right).$$

It is clear that the system now derived is still nonlinear, due to the dependence of the dynamics on the velocity and on the ranges. However, as both the first N_O ranges and the linear velocity are measured, the dependence of $\mathbf{A}_{RL}(\mathbf{x}_R(t), \mathbf{y}(t), t)$ in the full range state can be substituted by a dependence on the system output. This is done so that the observability analysis can be performed in a linear fashion, as it will be seen in the next section. Notice also that there are several singularities in the dynamics matrix, if one or more of the ranges becomes null. To prevent that, the following assumption is needed.

Assumption 1. *The motion of the vehicle is such that*

$$\underset{i\in\mathcal{L}}{\forall} \quad \underset{t\geq t_0}{\forall} \quad \underset{R_m, R_M>0}{\exists} : \quad R_m < r_i(t) < R_M.$$

Even though this assumption is needed for the dynamics matrix to be well-defined, it is straightforward to see that it is a very mild assumption, as, in practice, the vehicle is never coincident with a landmark nor can it be arbitrarily distant. Moreover, the values of R_m and R_M are not required for the filter design.

One final aspect important to retain is the fact that there is nothing in the system dynamics imposing the state relations expressed by (2), particularly the nonlinear relation $x_{R_i}(t) = \|\mathbf{x}_{L_i}(t)\|$. Although they could be established through augmented nonlinear outputs, that would invalidate the option to expand the system state in order to obtain a linear time-varying system. Furthermore, the next section presents a result that demonstrates that, in certain conditions, the dynamics of the system directly imposes these constraints.

3. Observability analysis

Before the RO-SLAM filter design can proceed properly, it is necessary to ensure observability of the derived system, and to validate theoretically the procedure of the state augmentation. This section addresses the observability analysis of the nonlinear system derived in the previous section, both in its original and augmented forms. Sufficient conditions for the observability of the system, with a physical insight on the motion of the vehicle, are obtained, and global convergence results are established.

Although the introduction of the augmented system (4) has removed the output nonlinearity existent in the original nonlinear system (1), the presence of the ranges to invisible landmarks in the dynamics matrix introduces another kind of problem. Furthermore, given that the only available information with which to obtain $\mathbf{x}_{L_i}(t)$ and $x_{R_i}(t)$ is the corresponding range, it is obvious that the invisible landmarks and their ranges cannot be observable. For this reason, and following the approach used in [26] and [25], the ranges to invisible landmarks and the landmarks themselves are removed from the system state, resulting in a reduced state, in which the dynamics matrix does not depend on the state as before, but solely on the system output. Thus, as the output is

known, this new system may be regarded as linear time-varying for observability purposes.

For the sake of simplicity, and without loss of generality, in this section it is assumed that there is only one visible landmark, i.e., $\mathcal{L}_O := \{1\}$. This is possible due to the multi-single-range character of the problem. Furthermore, as described, the invisible landmarks are discarded and left out of the new system state. Let $\mathbf{z}(t) = \begin{bmatrix}\mathbf{z}_{L_1}^T(t) & \mathbf{z}_V^T(t) & z_{R_1}(t)\end{bmatrix}^T$ be the new reduced state, and the corresponding system be

$$\begin{cases}\dot{\mathbf{z}}(t) = \mathbf{A}(t)\mathbf{z}(t) \\ \mathbf{y}(t) = \mathbf{C}\mathbf{z}(t)\end{cases} \tag{5}$$

where the dynamics matrix is given by

$$\mathbf{A}(t) := \begin{bmatrix}\mathbf{A}_{L_O}(t) & \mathbf{A}_{LV_O} & \mathbf{0}_{n_O \times n_R} \\ \mathbf{0}_{n_V \times n_O} & \mathbf{0}_{n_V} & \mathbf{0}_{n_V \times n_R} \\ \mathbf{A}_{RL_O}(t) & \mathbf{0}_{n_{R_O} \times n_V} & \mathbf{0}_{n_{R_O}}\end{bmatrix},$$

and the output matrix is simply

$$\mathbf{C} = \begin{bmatrix}\mathbf{0}_3 & \mathbf{I}_3 & \mathbf{0}_{3\times 1} \\ \mathbf{0}_{1\times 3} & \mathbf{0}_{1\times 3} & 1\end{bmatrix}.$$

Note that the blocks that constitute the dynamics matrix are the ones defined in the previous section, while including only the visible landmark. Also, the dependence on the system output and input can be seen as merely a dependence on time, as the two signals are known. This enables to consider (5) as a linear time-varying system (LTV), as shown in [23, Lemma 1]. This will be used throughout this section.

The following result addresses the observability analysis of the LTV system, but before proceeding with the analysis it is convenient to define ${}^I\mathbf{v}(t) = \mathbf{R}(t)\mathbf{v}(t)$ as the linear velocity of the vehicle in the inertial frame $\{I\}$.

Theorem 1. *Consider the LTV system given by* (5) *and let* $\mathcal{T} := [t_0, t_f]$. *If and only if there exist three instants* $\{t_1, t_2, t_3\} \in \mathcal{T}$ *such that the linear velocity of the vehicle expressed in the inertial frame is linearly independent in those instants, i.e.,* $\det\left(\begin{bmatrix}{}^I\mathbf{v}(t_1) & {}^I\mathbf{v}(t_2) & {}^I\mathbf{v}(t_3)\end{bmatrix}\right) \neq 0$, *then the system is observable in the sense that, given the system output* $\{\mathbf{y}(t),\, t \in \mathcal{T}\}$, *the initial condition* $\mathbf{z}(t_0)$ *is uniquely defined.*

Proof. The proof starts by transforming the LTV system through a Lyapunov transformation, to simplify the analysis. A Lyapunov transformation (see [29, Chapter 1, Section 8] for details), preserves the observability properties of the original system. Consider then the tranformation

$$\mathbf{T}(t) = \operatorname{diag}\left(\mathbf{R}(t), \mathbf{I}_3, 1\right),$$

and the transformed system state given by

$$\boldsymbol{\chi}(t) = \mathbf{T}(t)\mathbf{z}(t). \tag{6}$$

If it is considered that the angular velocity $\boldsymbol{\omega}(t)$ is bounded, which is a physically sound assumption, the transformation $\mathbf{T}(t)$ has a continuous and bounded time derivative, while also having a bounded determinant itself, and therefore it is indeed a Lyapunov transformation. This means that it suffices to prove that the transformed system is observable, an approach employed successfully in the past, in works such as [23].

Before proceeding with the proof it is necessary to derive the new system dynamics, by simply taking the first time derivative of (6) and using the inverse transformation $\mathbf{z}(t) = \mathbf{T}^{-1}(t)\boldsymbol{\chi}(t)$, which results in

$$\begin{cases} \dot{\boldsymbol{\chi}}(t) = \boldsymbol{\mathcal{A}}(t)\boldsymbol{\chi}(t) \\ \mathbf{y}(t) = \mathbf{C}\boldsymbol{\chi}(t) \end{cases}. \tag{7}$$

It is a simple matter of computation to see that the dynamics matrix of the transformed system is given by

$$\boldsymbol{\mathcal{A}}(t) = \begin{bmatrix} \mathbf{0}_3 & -\mathbf{R}(t) & \mathbf{0}_{3\times 1} \\ \mathbf{0}_3 & \mathbf{0}_3 & \mathbf{0}_{3\times 1} \\ -\frac{\mathbf{y}_v^T(t)}{y_{R_1}(t)}\mathbf{R}^T(t) & \mathbf{0}_{1\times 3} & 0 \end{bmatrix},$$

while the output matrix of the transformed system is the same as in (5).

The proof follows by computing the transition matrix of the transformed system and subsequently the observability Gramian that will help determine whether the system is observable or not. The computation of the transition matrix can be made either using the Peano-Baker series or, in this case, by simply solving

$$\boldsymbol{\phi}(t, t_0)\boldsymbol{\chi}(t_0) = \boldsymbol{\chi}(t_0) + \int_{t_0}^{t} \boldsymbol{\mathcal{A}}(\tau)\boldsymbol{\chi}(\tau)\mathrm{d}\tau.$$

The computed transition is given by

$$\boldsymbol{\phi}(t, t_0) = \begin{bmatrix} \mathbf{I}_3 & -\mathbf{R}^{[1]}(t, t_0) & \mathbf{0}_{3\times 1} \\ \mathbf{0}_3 & \mathbf{I}_3 & \mathbf{0}_{3\times 1} \\ -\mathbf{v}^{[0]}(t, t_0) & \mathbf{v}^{[1]}(t, t_0) & 1 \end{bmatrix}, \tag{8}$$

where the following auxiliary quantities are introduced to simplify this expression,

$$\begin{cases} \mathbf{R}^{[1]}(t, t_0) = \displaystyle\int_{t_0}^{t} \mathbf{R}(\tau)\mathrm{d}\tau \\ \mathbf{v}^{[0]}(t, t_0) = \displaystyle\int_{t_0}^{t} \frac{\mathbf{y}_v^T(\tau)}{y_{R_1}(\tau)}\mathbf{R}^T(\tau)\mathrm{d}\tau \\ \mathbf{v}^{[1]}(t, t_0) = \displaystyle\int_{t_0}^{t} \frac{\mathbf{y}_v^T(\tau)}{y_{R_1}(\tau)}\mathbf{R}^T(\tau)\mathbf{R}^{[1]}(\tau, t_0)\mathrm{d}\tau \end{cases}.$$

The observability Gramian is given by

$$\boldsymbol{\mathcal{W}}(t_0, t_f) = \int_{t_0}^{t_f} (\mathbf{C}\boldsymbol{\phi}(\tau, t_0))^T \mathbf{C}\boldsymbol{\phi}(\tau, t_0) \mathrm{d}\tau. \tag{9}$$

Consider again [23, Lemma 1]. If the observability Gramian now defined is invertible, then the transformed system is observable in the sense that, given the system output $\{\mathbf{y}(t), t \in \mathcal{T}\}$, the initial condition $\boldsymbol{\chi}(t_0)$ is uniquely defined. The proof follows by contraposition, i.e., by establishing the hypothesis that the system (7) is not observable and then showing that, if the conditions of the theorem apply, the hypothesis cannot hold. Suppose then that the system is unobservable. This, from the mentioned lemma, implies that $\boldsymbol{\mathcal{W}}(t_0, t_f)$ is singular, which means that there exists a unit vector $\mathbf{c} = \begin{bmatrix} \mathbf{c}_p^T & \mathbf{c}_v^T & c_r \end{bmatrix}^T \in \mathbb{R}^{n_\chi}$ such that

$$\mathbf{c}^T \boldsymbol{\mathcal{W}}(t_0, t_f)\mathbf{c} = 0. \tag{10}$$

Then, the substitution of (9) in (10) yields

$$\mathbf{c}^T \boldsymbol{\mathcal{W}}(t_0, t_f)\mathbf{c} = \int_{t_0}^{t_f} \|\mathbf{C}\boldsymbol{\phi}(\tau, t_0)\mathbf{c}\|^2 \mathrm{d}\tau, \tag{11}$$

where it is possible to substitute the argument of the norm in the integral by a vector function $\mathbf{f}(\tau, t_0)$ such that $\mathbf{f}(\tau, t_0) = \mathrm{diag}\left(\mathbf{R}^T(\tau), 1\right) \mathbf{C}\boldsymbol{\phi}(\tau, t_0)\mathbf{c}$. Note
210 that $\|\mathbf{f}(\tau, t_0)\| = \|\mathbf{C}\boldsymbol{\phi}(\tau, t_0)\mathbf{c}\|$.

In order for (10) to be true, both $\mathbf{f}(\tau, t_0)$ and its derivative must be zero for all $\tau \in \mathcal{T}$. Consider now the expressions for these two quantities, given by

$$\mathbf{f}(\tau, t_0) = \begin{bmatrix} \mathbf{c}_v \\ f_r(\tau, t_0) \end{bmatrix} \tag{12}$$

and

$$\frac{\mathrm{d}}{\mathrm{d}\tau}\mathbf{f}(\tau, t_0) = \begin{bmatrix} \mathbf{0}_{3\times 1} \\ \frac{\mathrm{d}}{\mathrm{d}\tau} f_r(\tau, t_0) \end{bmatrix} \tag{13}$$

respectively. The component of $\mathbf{f}(\tau, t_0)$ associated with the range output is given by

$$f_r(\tau, t_0) = -\mathbf{v}^{[0]}(\tau, t_0)\mathbf{c}_p + \mathbf{v}^{[1]}(\tau, t_0)\mathbf{c}_v + c_r,$$

while its derivative is

$$\frac{\mathrm{d}}{\mathrm{d}\tau} f_r(\tau, t_0) = -\frac{\mathbf{y}_v^T(\tau)\mathbf{R}^T(\tau)}{y_{R_1}(\tau)}\mathbf{c}_p + \frac{\mathbf{y}_v^T(\tau)\mathbf{R}^T(\tau)}{y_{R_1}(\tau)}\mathbf{R}^{[1]}(\tau, t_0)\mathbf{c}_v.$$

Evaluating (12) at $\tau = t_0$ while equating the result to zero, automatically wields $\mathbf{c}_v = \mathbf{0}$ and $c_r = 0$. Furthermore, for (10) to be true, $\frac{\mathrm{d}}{\mathrm{d}\tau}\mathbf{f}(\tau, t_0)$ must be zero. This, recalling Assumption 1, leads to the final condition, expressed by

$${}^I\mathbf{v}^T(\tau)\ \mathbf{c}_p = 0,\ \forall \tau \in \mathcal{T}.$$

This condition can only be satisfied if $\mathbf{c}_p = \mathbf{0}$, which contradicts the hypothesis of the proof ($\|\mathbf{c}\| = 1$), or if the linear velocity of the vehicle in the inertial frame for any t_1, t_2, and t_3 in $\mathcal{T}$ is such that

$$\det\left(\begin{bmatrix} {}^I\mathbf{v}^T(t_1) \\ {}^I\mathbf{v}^T(t_2) \\ {}^I\mathbf{v}^T(t_3) \end{bmatrix}\right) = 0,$$

i.e., there do not exist three time instants such that the linear velocity of the vehicle in $\{I\}$ on these instants spans $\mathbb{R}^3$, which contradicts the conditions of the theorem. Therefore, by contraposition, if the conditions of the theorem hold, then $\boldsymbol{\mathcal{W}}(t_0, t_f)$ is invertible on $\mathcal{T}$, and, using [23, Lemma 1], it follows that (7) is observable. Furthermore, the LTV system (5) is also observable, as it is related with the system (7) through a Lyapunov transformation, thus concluding the sufficiency part of the proof.

The proof that the observability of the system implies that the conditions of the theorem hold, i.e., the necessity of those conditions, is also done by contraposition. It is assumed that the conditions of the theorem do not hold, and it is shown that, in this case, the system is not observable. Consider then that the conditions of the theorem do not hold. Therefore, the vehicle can only move in a plane or a line, which means that the inertial velocity vector is always in the same plane, i.e.,

$${}^I\mathbf{v}(t) = v_\gamma(t)\boldsymbol{\gamma} + v_\nu(t)\boldsymbol{\nu}, \quad \forall t \in \mathcal{T} \tag{14}$$

where $v_\gamma(t)$ and $v_\nu(t) \in \mathbb{R}$, and $\boldsymbol{\gamma}$ and $\boldsymbol{\nu}$ are two orthonormal vectors in $\mathbb{R}^3$ that define the plane or line (case defined by $v_\nu(t) = 0$) in which the vehicle moves. The computation of the explicit evolution of the output of the system (7) as a function of the initial state $\boldsymbol{\chi}(t_0)$ is needed to proceed with the proof. Recall the definition of the transition matrix in (8) and the output in (7), which combined yield $\mathbf{y}(t) = \mathbf{C}\boldsymbol{\phi}(t, t_0)\boldsymbol{\chi}(t_0)$ or

$$\mathbf{y}(t) = \begin{bmatrix} \boldsymbol{\chi}_V(t_0) \\ -\mathbf{v}^{[0]}(t, t_0)\boldsymbol{\chi}_L(t_0) + \mathbf{v}^{[1]}(t, t_0)\boldsymbol{\chi}_V(t_0) + \chi_R(t_0) \end{bmatrix}.$$

The scalar part of the output can be further expanded to read

$$y_R(t) = \chi_R(t_0) + \mathbf{v}^{[1]}(t, t_0)\boldsymbol{\chi}_V(t_0) - \int_{t_0}^{t} \frac{\mathbf{y}_v^T(\tau)\mathbf{R}^T(\tau)}{y_R(\tau)}\boldsymbol{\chi}_L(t_0)\mathrm{d}\tau, \tag{15}$$

and substituting (14) in (15) leads to

$$\begin{aligned} y_R(t) = \chi_R(t_0) + \mathbf{v}^{[1]}(t, t_0)\boldsymbol{\chi}_V(t_0) &- \int_{t_0}^{t} \frac{v_\gamma(\tau)}{y_R(\tau)}\mathrm{d}\tau\, \boldsymbol{\gamma} \cdot \boldsymbol{\chi}_L(t_0) \\ &- \int_{t_0}^{t} \frac{v_\nu(\tau)}{y_R(\tau)}\mathrm{d}\tau\, \boldsymbol{\nu} \cdot \boldsymbol{\chi}_L(t_0). \end{aligned} \tag{16}$$

The observability of the system implies that any two different initial states are distinguishable using only the output, i.e., if two different initial states produce the same output, the system cannot be observable. The proof follows by choosing two particular examples of initial states that produce the same output for all time. For that purpose, consider the two initial conditions

$$\tilde{\boldsymbol{\chi}}(t_0) = \begin{bmatrix} \boldsymbol{\chi}_V^T(t_0) & (\boldsymbol{\nu} \times \boldsymbol{\gamma})^T & \chi_R(t_0) \end{bmatrix}^T$$

and

$$\bar{\boldsymbol{\chi}}(t_0) = \begin{bmatrix} \boldsymbol{\chi}_V^T(t_0) & (\boldsymbol{\gamma} \times \boldsymbol{\nu})^T & \chi_R(t_0) \end{bmatrix}^T .$$

Observe that the range state $\chi_R(t_0)$ is the same for both initial states, which makes sense, as $\|\boldsymbol{\nu} \times \boldsymbol{\gamma}\| = \|\boldsymbol{\gamma} \times \boldsymbol{\nu}\|$. Noting that $\boldsymbol{\nu} \cdot (\boldsymbol{\nu} \times \boldsymbol{\gamma}) = 0$ and $\boldsymbol{\gamma} \cdot (\boldsymbol{\nu} \times \boldsymbol{\gamma}) = 0$, it is straightforward to see that the two integrals in (16) vanish for these two initial states, rendering the output equal in both cases, i.e., $\tilde{\boldsymbol{\chi}}(t_0)$ and $\bar{\boldsymbol{\chi}}(t_0)$ are indistinguishable, as they lead to the same output for all $t \in \mathcal{T}$. Hence, if the conditions of the theorem do not hold, it is possible to find at least two indistinguishable initial states, which means that the transformed system (7) is unobservable in $\mathcal{T}$, or, conversely, if the transformed system is observable the theorem conditions must hold. As the two LTV systems are related by the Lyapunov transformation (6) which preserves observability properties, the proof of the necessity of those conditions is concluded. □

Remark 1. *This theorem establishes requirements for the motion of the vehicle, as it allows to conclude that if there are at least three velocity vectors that span* $\mathbb{R}^3$*, or, equivalently, if the trajectory of the vehicle is not restricted to a line or a plane, the system is observable. Note that, in a trilateration technique, ranges to four non-coplanar vehicle positions are needed. In this system, the motion of the vehicle provides those positions as Fig. 1 shows for the bidimensional case (chosen for better visualization).*

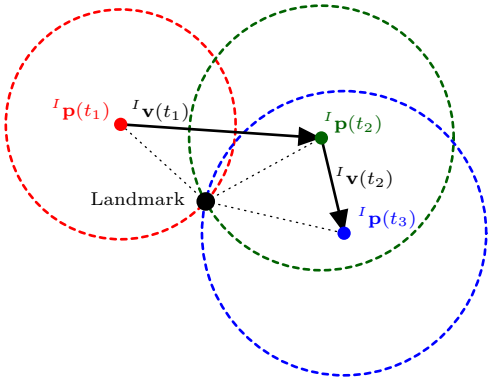

Figure 1: Trilateration for positioning a landmark in 2-D.

The LTV system (5) is a reduction of the augmented nonlinear system (4) in the sense that it does not include the invisible landmarks, and assumes the existence of only a single visible landmark. Due to the independence of the landmarks, whichever their number is, the two systems are completely equivalent in terms of observability, discarding the invisible landmarks. Note that the observability result of Theorem 1 when applied to the multi landmark case requires each landmark to be visible in the time instants when the velocity spans $\mathbb{R}^3$. This does not mean that all landmarks must be visible at the same time, but that in the time intervals in which each landmark is visible the conditions of Theorem 1 must hold. Furthermore, care must be taken before extending the observability results of this section to the original nonlinear system (1). As there is nothing imposing the state relations (2), it is not possible to apply the results to the original nonlinear system without some reflection. The following result addresses this issue: firstly, the equivalence of the state of the nonlinear and LTV systems is performed in a similar fashion to what was done in [23] and [28]. Secondly, it is shown that the nonlinear relation $\mathbf{z}_{R_1}(t) = \|\mathbf{z}_{L_1}\|$ is automatically imposed by the system dynamics when the LTV system is observable.

Theorem 2. *Consider the LTV system* (5) *and the original nonlinear system* (1)*. If the conditions of Theorem 1 hold, then*

(i) the state of the original nonlinear system and that of the LTV system are the same and uniquely defined, provided that the invisible landmarks are discarded. Furthermore the constraints expressed by (2) *become naturally imposed by the dynamics; and*

(ii) a state observer with uniformly globally exponentially stable error dynamics for the LTV system is also a state observer for the underlying nonlinear system, and the estimation error converges exponentially fast for all initial conditions.

Proof. The proof of the first part of the theorem follows by considering the system output and its relation to the states of the two systems in analysis, leading to a series of equations which, in the conditions of the theorem, result in the correspondence between the states, while imposing the algebraic constraints.

Consider the output of the LTV system (5), given by $\mathbf{y}(t) = \mathbf{C}\mathbf{z}(t)$, and that of the original nonlinear system, $\mathbf{y}(t) = \begin{bmatrix}\mathbf{v}^T(t) & \|\mathbf{p}_1(t)\|\end{bmatrix}^T$. Recall that, in this section, it is assumed that the visible landmark set has only one landmark. The comparison of the two outputs shows that

$$\begin{cases} \mathbf{z}_V(t) = \mathbf{v}(t) \\ z_{R_1}(t) = \|\mathbf{p}_1(t)\| \end{cases}.$$

For the purpose of finding the correspondence of the remaining states, $\mathbf{z}_{L_1}(t)$ and $\mathbf{p}_1(t)$, consider the time evolution of the rotation of each of these states, given by

$$\mathbf{R}(t)\mathbf{z}_{L_1}(t) = \mathbf{R}(t_0)\mathbf{z}_{L_1}(t_0) - \mathbf{R}^{[1]}(t, t_0)\mathbf{z}_V(t_0), \tag{17}$$

and

$$\mathbf{R}(t)\mathbf{p}_1(t) = \mathbf{R}(t_0)\mathbf{p}_1(t_0) - \mathbf{R}^{[1]}(t,t_0)\mathbf{v}(t_0), \tag{18}$$

respectively. These can be derived following the same reasoning used to compute the transition matrix (8). The expressions in (17) and (18) can be used to compute the derivative of the outputs of the two systems in analysis related to the ranges. Recall that the range output of the LTV system is the same as the range state of that system. Then, using the dynamics of that state given by

$$\dot{z}_{R_1}(t) = -\frac{\mathbf{y}_v^T(t)}{y_{R_1}(t)}\mathbf{z}_{L_1}(t),$$

replacing $\mathbf{z}_{L_1}(t)$ by $\mathbf{R}^T(t)\mathbf{R}(t)\mathbf{z}_{L_1}(t)$, and using (17) yields

$$\dot{y}_{R_1}(t) = \frac{\mathbf{y}_v^T(t)\mathbf{R}^T(t)}{y_{R_1}(t)}\left(\mathbf{R}(t_0)\mathbf{z}_{L_1}(t_0) - \mathbf{R}^{[1]}(t,t_0)\mathbf{z}_V(t_0)\right). \tag{19}$$

For the original system, recall the derivative of the range output given by (3), and substitute $\mathbf{p}_1(t)$ by $\mathbf{R}^T(t)\mathbf{R}(t)\mathbf{p}_1(t)$ in order to be able to use (18) and reach

$$\dot{r}_1(t) = \frac{\mathbf{v}^T(t)\mathbf{R}^T(t)}{r_1(t)}\left(\mathbf{R}(t_0)\mathbf{p}_1(t_0) - \mathbf{R}^{[1]}(t,t_0)\mathbf{v}(t_0)\right). \tag{20}$$

It is possible to compare these two expressions for the derivatives of the outputs of the two systems, if it is noted that $\mathbf{z}_V(t) = \mathbf{v}(t)$, $r_1(t) = y_{R_1}(t)$, and ${}^I\mathbf{v}(t) = \mathbf{R}(t)\mathbf{y}_v(t) = \mathbf{R}(t)\mathbf{v}(t)$. Then, the comparison of (19) with (20) yields

$$\frac{{}^I\mathbf{v}^T(t)}{r_1(t)}\mathbf{R}(t_0)\left(\mathbf{z}_{L_1}(t_0) - \mathbf{p}_1(t_0)\right) = 0$$

for all t in $\mathcal{T}$. When the conditions of Theorem 1 hold, this expression implies $\mathbf{z}_{L_1}(t_0) = \mathbf{p}_1(t_0)$ by the same reasoning used to prove the sufficiency of these conditions to the observability of the LTV system. Since the dynamics of these states are the same by construction, the equivalence of the initial conditions implies that the system states are equivalent. Hence, if the conditions for the observability of the LTV system apply, then the state of the system (5) corresponds directly to that of the original nonlinear system, disregarding the invisible landmarks. Furthermore, noting that it is imposed by the output that $z_{R_1}(t)$ is the norm of $\mathbf{p}_1(t)$ and, if the conditions of the theorem hold, that $\mathbf{p}_1(t) = \mathbf{z}_{L_1}(t)$, then the constraint $z_{R_1}(t) = \|\mathbf{z}_{L_1}(t)\|$ becomes naturally imposed by the dynamics. Thus, the proof of the first part of the theorem is concluded.

The second part of the theorem follows naturally from the first part. An observer for (5) with globally exponentially stable error dynamics provides estimates that converge exponentially fast to the true state. Therefore, if the state of the LTV system and that of the original nonlinear system, when the invisible landmarks are discarded, are one and the same, the estimates of the observer will also tend exponentially fast to the true state of system (1) with the same error dynamics. □

Theorems 1 and 2 provided sufficient conditions for the observability of the original nonlinear system while establishing a direct relation between the augmented system 5 and the nonlinear one. However, a stronger result can be accomplished by means of the following theorem, which states that these conditions are indeed necessary and sufficient.

Theorem 3. *The nonlinear system* (1) *is observable, when discarding the invisible landmarks, if and only if the conditions of Theorem 1 hold.*

Proof. The sufficiency part of the proof is readily provided by Theorems 1 and 2. The former establishes conditions for the observability of the LTV system (5) and the latter relates the state of that system to that of the nonlinear system in analysis. The proof of the necessity part of the theorem is made in very similar terms to that of the second part of Theorem 1 in the sense that the system output, written as a function of the initial state using (18)

$$\begin{aligned} r_1(t) &= \|\mathbf{R}(t)\mathbf{p}_1(t)\| \\ &= \|\mathbf{R}(t_0)\mathbf{p}_1(t_0) - \mathbf{R}^{[1]}(t,t_0)\mathbf{v}(t_0)\|, \end{aligned}$$

is shown to be the same given two different initial states. Squaring this expression and expanding the result yields

$$\begin{aligned} r_1^2(t) = \|\mathbf{R}(t_0)\mathbf{p}_1(t_0)\|^2 + \|\mathbf{R}^{[1]}(t,t_0)\mathbf{v}(t_0)\|^2 \\ - 2\int_{t_0}^{t} \left(v_\gamma(\tau)\boldsymbol{\gamma} + v_\nu(\tau)\boldsymbol{\nu}\right)\mathbf{R}(t_0)\mathbf{p}_1(t_0)\mathrm{d}\tau, \quad (21) \end{aligned}$$

where the definition of $\mathbf{R}^{[1]}(t,t_0)$ and ${}^I\mathbf{v}(\tau) = \mathbf{R}(\tau)\mathbf{v}(t_0)$ were employed. Furthermore, the linear velocity in $\{I\}$ was also replaced in (21) by the negation of the conditions of the theorem expressed by (14). Consider two initial states defined as

$$\tilde{\boldsymbol{\xi}}(t_0) = \begin{bmatrix} \mathbf{R}^T(t_0)\left(\boldsymbol{\gamma}\times\boldsymbol{\nu}\right) \\ \mathbf{v}(t_0) \end{bmatrix}$$

and

$$\bar{\boldsymbol{\xi}}(t_0) = \begin{bmatrix} \mathbf{R}^T(t_0)\left(\boldsymbol{\nu}\times\boldsymbol{\gamma}\right) \\ \mathbf{v}(t_0) \end{bmatrix}.$$

Then, it is possible to see that the integral in (21) vanishes for both cases, and that these two initial states lead to the same output, which implies that if the conditions of the theorem do not hold, the system is unobservable. This concludes the proof of the necessity of the conditions of the theorem for the nonlinear system to be observable. □

The previous results show that, if it is possible to design a globally exponentially stable observer for the LTV system, it will also be suitable for the original

nonlinear system. This has established the ground to the design of such an observer, using a linear time-varying Kalman filter, which, to assure the GES nature of the estimation error dynamics, requires the pair $(\mathbf{A}(t), \mathbf{C})$ to be uniformly completely observable. This can be shown using the Lyapunov function $V(t, \tilde{\mathbf{z}}) = \tilde{\mathbf{z}}^T(t)\mathbf{P}^{-1}(t)\tilde{\mathbf{z}}(t)$, where $\tilde{\mathbf{z}}(t)$ is the observer error and $\mathbf{P}(t)$ is the error covariance and demonstrating that it respects all the conditions of [30, Theorem 8.5] for global exponential stability. The steps taken are similar to the ones in [30, Example 8.5] and include showing that $\mathbf{P}^{-1}(t)$ is positive definite using several results of [31]. The following theorem addresses the uniform complete observability of the pair $(\mathbf{A}(t), \mathbf{C})$. However, an additional assumption on the linear velocity of the vehicle is required.

Assumption 2. *The norm of the linear velocity of the vehicle in the inertial frame $\{I\}$ is always bounded, i.e.,*

$$\underset{t\geq t_0}{\forall} \quad \underset{V_M>0}{\exists} : \quad \|{}^I\mathbf{v}(t)\| \leq V_M.$$

Although imposing definite bounds on the linear velocity, this assumption is still a mild one, as it is physically impossible to reach arbitrarily large speeds. Moreover, the value of V_M is not required for the filter design.

Theorem 4. *The pair $(\mathbf{A}(t), \mathbf{C})$ is uniformly completely observable if and only if Assumption 2 is true and there exist $\delta > 0$ and $\alpha^* > 0$ such that, for all $t \geq t_0$, it is possible to choose a set of instants $\{t_1, t_2, t_3\} \in \mathcal{T}_\delta$, with $\mathcal{T}_\delta := [t, t+\delta]$, for which the linear velocity of the vehicle in the inertial frame respects*

$$\left|\det\left(\begin{bmatrix} {}^I\mathbf{v}(t_1) & {}^I\mathbf{v}(t_2) & {}^I\mathbf{v}(t_3)\end{bmatrix}\right)\right| > \alpha^*. \tag{22}$$

Proof. The concept of uniform complete observability implies uniform bounds on the observability Gramian in time intervals of length δ. Considering that the pair $(\mathbf{A}(t), \mathbf{C})$ is related to $(\boldsymbol{\mathcal{A}}(t), \mathbf{C})$ by a Lyapunov transformation, the uniform complete observability of the latter implies the uniform complete observability of the former, and thus the proof will focus on this pair.

Consider the previous definitions of the observability Gramian in (9) and of the arbitrary unitary vector $\mathbf{c}$, and note that these are bounded. Then, the uniform complete observability of the pair $(\boldsymbol{\mathcal{A}}(t), \mathbf{C})$ may be expressed through the following statement,

$$\underset{\substack{\delta>0\\ \alpha>0}}{\exists} \quad \underset{t\geq t_0}{\forall} \quad \underset{\substack{\mathbf{c}\in\mathbb{R}^{n_\mathcal{X}}\\ \|\mathbf{c}\|=1}}{\forall} : \quad \mathbf{c}^T\boldsymbol{\mathcal{W}}(t, t+\delta)\mathbf{c} \geq \alpha. \tag{23}$$

The proof follows by exhaustion, i.e., it consists of studying $\mathbf{c}^T\boldsymbol{\mathcal{W}}(t, t+\delta)\mathbf{c}$ for every possible case of $\mathbf{c}$ and showing that (23) is true for all of them.

Recall the proof of Theorem 1, and the expansion of $\mathbf{c}^T\boldsymbol{\mathcal{W}}(t_0, t_f)\mathbf{c}$ therein, with the definition of $\mathbf{f}(\tau, t)$ and $\frac{\mathrm{d}}{\mathrm{d}\tau}\mathbf{f}(\tau, t)$ in (12) and (13). Then, it is possible to write

$$\|\mathbf{f}(\tau, t)\|^2 = \|\mathbf{c}_v\|^2 + \left(\mathbf{v}^{[0]}(\tau, t)\mathbf{c}_p - \mathbf{v}^{[1]}(\tau, t)\mathbf{c}_v - c_r\right)^2. \tag{24}$$

[32, Proposition 4.2] is of great importance in the establishment of the result of this theorem. It states that if it is possible to find a positive constant β such that $\|\frac{\partial^i}{\partial\tau^i}\mathbf{g}(\tau,t_0)\| \geq \beta$ then there exists a $\gamma > 0$ such that $\|\mathbf{g}(t_0,t_0+\delta)\| \geq \gamma$ as long as $\frac{\partial^j}{\partial\tau^j}\mathbf{g}(\tau,t_0)|_{\tau=t_0} = 0$ for all $j < i$ and the norm of the $(i+1)$-th derivative is upper bounded. It is possible to see that this proposition applies to $\mathbf{c}^T\boldsymbol{\mathcal{W}}(t_0,t_f)\mathbf{c}$, and therefore it suffices to show that $\|\mathbf{f}(\tau,t)\|$ is lower bounded for every possible $\mathbf{c}$.

The first condition to study is $\|\mathbf{c}_v\| \geq \alpha_v > 0$ without any restriction on both $\mathbf{c}_p$ or c_r. In that case, the norm of $\mathbf{f}(\tau,t)$ respects

$$\|\mathbf{f}(\tau,t)\| \geq \|\mathbf{c}_v\| \geq \alpha_v,$$

and thus $\mathbf{c}^T\boldsymbol{\mathcal{W}}(t,t+\delta)\mathbf{c} \geq \alpha_1 > 0$. The second case is $|c_r| \geq \alpha_r > 0$, again with no restriction on the remaining quantities. Then, it is possible to evaluate $\mathbf{f}(\tau,t)$ for $\tau = t$ which leads to

$$\|\mathbf{f}(t,t)\| \geq |c_r| \geq \alpha_r.$$

The last case involves setting $\|\mathbf{c}_v\| < \alpha_v$ and $|c_r| < \alpha_r$, while imposing $\|\mathbf{c}_p\| \geq \alpha_p > 0$. For the purpose of analysing this case, consider the new function

$$f_{pv}(\tau,t) := \mathbf{v}^{[0]}(\tau,t)\mathbf{c}_p - \mathbf{v}^{[1]}(\tau,t)\mathbf{c}_v$$

such that $f_r(\tau,t) = -f_{pv}(\tau,t) + c_r$. Then, it is possible to write

$$\begin{aligned}\|\mathbf{f}(\tau,t)\|^2 &\geq f_r^2(\tau,t)\\ &\geq |f_{pv}(\tau,t)|(|f_{pv}(\tau,t)| - 2|c_r|)\\ &\geq |f_{pv}(\tau,t)|(|f_{pv}(\tau,t)| - 2\alpha_r).\end{aligned}$$

Considering that $f_{pv}(\tau,t)$ is lower bounded by some α_{pv}, if the upper bound on c_r is chosen to be smaller than $\frac{1}{4}\alpha_{pv}$, then

$$\|\mathbf{f}(\tau,t)\|^2 \geq \frac{\alpha_{pv}^2}{2},$$

and it suffices to show that the norm of the function $f_{pv}(\tau,t)$ is lower bounded. Then, one has $f_{pv}(t,t) = 0$, and [32, Proposition 4.2] applies once more, i.e., if it is shown that $\left|\frac{\mathrm{d}}{\mathrm{d}\tau}f_{pv}(\tau,t)\right| \geq \alpha_2$, then $\|\mathbf{f}(\tau,t)\|$ is lower bounded as intended. The norm of the derivative of $f_{pv}(\tau,t)$ is given by

$$\left|\frac{\mathrm{d}}{\mathrm{d}\tau}f_{pv}(\tau,t)\right| = \left|\frac{{}^I\mathbf{v}^T(\tau)}{r_1(\tau)}\mathbf{c}_p - \frac{{}^I\mathbf{v}^T(\tau)}{r_1(\tau)}\mathbf{R}^{[1]}(\tau,t)\mathbf{c}_v\right|, \tag{25}$$

where, in the definitions of $\mathbf{v}^{[0]}(\tau,t)$ and $\mathbf{v}^{[1]}(\tau,t)$, $\mathbf{R}(\tau)\mathbf{y}_v(\tau)$ was replaced by ${}^I\mathbf{v}(\tau)$ and $y_{R_1}(\tau)$ by $r_1(\tau)$. The square of (25) can be expanded to read

$$\begin{aligned}\left|\frac{\mathrm{d}}{\mathrm{d}\tau}f_{pv}(\tau,t)\right|^2 = \left|\frac{{}^I\mathbf{v}^T(\tau)}{r_1(\tau)}\mathbf{c}_p\right|^2 + \left|\frac{{}^I\mathbf{v}^T(\tau)}{r_1(\tau)}\mathbf{R}^{[1]}(\tau,t)\mathbf{c}_v\right|^2\\ - 2\frac{{}^I\mathbf{v}^T(\tau)}{r_1(\tau)}\mathbf{c}_p\frac{{}^I\mathbf{v}^T(\tau)}{r_1(\tau)}\mathbf{R}^{[1]}(\tau,t)\mathbf{c}_v.\end{aligned}$$

Consider now Assumptions 1 and 2. Using the bounds defined therein, it is possible to write

$$\left|\frac{\mathrm{d}}{\mathrm{d}\tau}f_{pv}(\tau,t)\right|^2 \geq \left|\frac{{}^I\mathbf{v}^T(\tau)}{r_1(\tau)}\mathbf{c}_p\right|\left(\left|\frac{{}^I\mathbf{v}^T(\tau)}{r_1(\tau)}\mathbf{c}_p\right| - 2\frac{\|{}^I\mathbf{v}(t)\|\|\mathbf{c}_v\|}{r_1(\tau)}\right)$$
$$\geq \frac{\left|{}^I\mathbf{v}^T(\tau)\mathbf{c}_p\right|}{R_M^2}\left(\left|{}^I\mathbf{v}^T(\tau)\mathbf{c}_p\right| - 2\frac{R_M V_M \alpha_v}{R_m}\right).$$

Assuming that $\left|{}^I\mathbf{v}^T(\tau)\mathbf{c}_p\right| \geq \alpha_3$ for some τ, if it is defined that $\alpha_v < \frac{R_m}{4R_M V_M}\alpha_3$, then the norm of this derivative respects

$$\left|\frac{\mathrm{d}}{\mathrm{d}\tau}f_{pv}(\tau,t)\right|^2 \geq \frac{1}{2R_M^2}\alpha_3^2.$$

The proof follows now by showing that there is at least a t^* such that the absolute value of the inner product of the linear velocity in $\{I\}$ with $\mathbf{c}_p$ in that instant is greater than some α_3 for all $\|\mathbf{c}_p\| \geq \alpha_p$. Consider the sum of the mentioned inner product for the time instants t_1, t_2, and t_3. Given that $\mathbf{c}_p$ cannot be perpendicular to all velocities, as it is impossible according to the conditions of the theorem, the worst case occurs when $\mathbf{c}_p$ is perpendicular to the two velocity vectors that have the greatest cross product, say ${}^I\mathbf{v}(t_2)$ and ${}^I\mathbf{v}(t_3)$. The condition of the theorem can be written as

$$\left|{}^I\mathbf{v}^T(t_1)\mathbf{S}\left[{}^I\mathbf{v}(t_2)\right]{}^I\mathbf{v}(t_3)\right| \geq \alpha. \tag{26}$$

In the worst case now defined, $\mathbf{c}_p = \pm\frac{\mathbf{S}\left[{}^I\mathbf{v}(t_2)\right]{}^I\mathbf{v}(t_3)}{\|\mathbf{S}\left[{}^I\mathbf{v}(t_2)\right]{}^I\mathbf{v}(t_3)\|}\|\mathbf{c}_p\|$, which can be substituted in (26) to yield

$$\left|{}^I\mathbf{v}^T(t_1)\mathbf{c}_p\right| \geq \alpha\frac{\alpha_p}{V_M^2}.$$

Hence, in the conditions of the theorem, the sum of the absolute values of the inner products of the linear velocity in $\{I\}$ with $\mathbf{c}_p$ at t_1, t_2, and t_3 respects

$$\sum_{i=1}^{3}\left|{}^I\mathbf{v}^T(t_i)\mathbf{c}_p\right| \geq \alpha\frac{\alpha_p}{V_M^2}.$$

This means that there exists at least a t^* equal to t_1, t_2, t_3 or any combination of the three such that

$$\left|{}^I\mathbf{v}^T(t^*)\mathbf{c}_p\right| \geq \alpha\frac{\alpha_p}{3V_M^2},$$

which implies that

$$\left|\frac{\mathrm{d}}{\mathrm{d}\tau}f_{pv}(t^*,t)\right| \geq \frac{\alpha\alpha_p}{3\sqrt{2}R_M V_M^2},$$

and, by [32, Proposition 4.2], $|f_{pv}(\tau,t)| \geq \alpha_3$, which in turn implies $\|\mathbf{f}(\tau,t)\| \geq \alpha_4$.

This concludes the enumeration of all the possible values for $\mathbf{c}$, and the proof that, for every possibility, $\mathbf{c}^T\boldsymbol{\mathcal{W}}(t,t+\delta)\mathbf{c}$ is lower bounded, thus proving the sufficiency of the conditions of the theorem for the uniform complete observability of the pair $(\boldsymbol{\mathcal{A}}(t),\mathbf{C})$. Being related to the LTV system (5) through a Lyapunov transformation, this result implies that $(\mathbf{A}(t),\mathbf{C}(t))$ is also uniformly completely observable, and thus the proof of the sufficiency part of the theorem is concluded.

In the same manner of the previous necessity theorems, the proof is made by contraposition, i.e, by showing that the negation of the conditions implies that the pair $(\mathbf{A}(t),\mathbf{C})$ cannot be uniformly completely observable. Consider then the negation of the conditions of the theorem, stated by

$$\underset{\substack{\delta>0\\ \alpha>0}}{\forall}\ \underset{t\geq t_0}{\exists}\ \underset{t_1,t_2,t_3\in\mathcal{T}_\delta}{\forall}: \quad \left|\det\left(\begin{bmatrix} {}^I\mathbf{v}^T(t_1)\\ {}^I\mathbf{v}^T(t_2)\\ {}^I\mathbf{v}^T(t_3)\end{bmatrix}\right)\right|<\alpha \quad \text{or} \quad \text{Assumption 2 is false.}$$

This means that the linear velocity of the vehicle in the inertial frame can move in $\mathbb{R}^3$ even though the quality of the tridimensional space it spans is degraded, i.e., considering that the inertial linear velocity is, in general, given by ${}^I\mathbf{v}(t)=v_\gamma(t)\boldsymbol{\gamma}+v_\nu(t)\boldsymbol{\nu}+v_\rho(t)\boldsymbol{\rho}$, there is at least one direction $\boldsymbol{\rho}$ in $\mathbb{R}^3$ upon which the linear velocity is upper bounded and as small as wanted, $|{}^I\mathbf{v}(t)\cdot\boldsymbol{\rho}|<\beta$ for all $t\in\mathcal{T}_\delta$ and for all $\beta>0$. The proof follows by showing that this limitation on the linear velocity implies that the pair $(\boldsymbol{\mathcal{A}}(t),\mathbf{C})$ is not uniformly completely observable, i.e.,

$$\underset{\substack{\delta>0\\ \epsilon>0}}{\forall}\ \underset{t\geq t_0}{\exists}\ \underset{\substack{\mathbf{c}\in\mathbb{R}^{n_\mathbf{X}}\\ \|\mathbf{c}\|=1}}{\exists}: \quad \mathbf{c}^T\boldsymbol{\mathcal{W}}(t,t+\delta)\mathbf{c}<\epsilon. \tag{27}$$

For that purpose, consider the substitution of (24) in the definition of $\mathbf{c}^T\boldsymbol{\mathcal{W}}(t,t+\delta)\mathbf{c}$ given by (11), which yields

$$\mathbf{c}^T\boldsymbol{\mathcal{W}}(t,t_0)\mathbf{c}=\int_t^{t+\delta}\|\mathbf{c}_v\|^2\mathrm{d}\tau+\int_t^{t+\delta}\left(\mathbf{v}^{[0]}(\tau,t)\mathbf{c}_p-\mathbf{v}^{[1]}(\tau,t)\mathbf{c}_v-c_r\right)^2\mathrm{d}\tau. \tag{28}$$

The statement (27) requires the existence of a single unit vector $\mathbf{c}$ that satisfies it. Therefore, it is possible to choose particular values for $\mathbf{c}_p$, $\mathbf{c}_v$, and c_r that aid the development of the proof. For that purpose, consider that $\mathbf{c}_v$ and c_r are both zero. In this case, (28) becomes

$$\mathbf{c}^T\boldsymbol{\mathcal{W}}(t,t+\delta)\mathbf{c}=\int_t^{t+\delta}\left[\int_t^{\tau}\frac{\mathbf{y}_v^T(\sigma)\mathbf{R}^T(\sigma)}{y_{R_1}(\sigma)}\mathbf{c}_p\mathrm{d}\sigma\right]^2\mathrm{d}\tau,$$

which, noting that ${}^I\mathbf{v}(t)=\mathbf{R}(t)\mathbf{y}_v(t)$ and $y_{R_1}(t)=r_1(t)$ and using the Cauchy-Schwartz inequality, allows to write

$$\mathbf{c}^T\boldsymbol{\mathcal{W}}(t,t+\delta)\mathbf{c}\leq\int_t^{t+\delta}\int_t^{\tau}\left[\frac{{}^I\mathbf{v}^T(\sigma)\mathbf{c}_p}{r_1(\sigma)}\right]^2\mathrm{d}\sigma\mathrm{d}\tau.$$

If $\mathbf{c}_p$ is chosen as the unit vector $\boldsymbol{\rho}$ previously introduced, it is possible to further simplify this expression, yielding

$$\underset{\substack{\delta>0\\ \epsilon>0}}{\forall} \quad \underset{t\geq t_0}{\exists} \quad \underset{\substack{\mathbf{c}\in\mathbb{R}^{n_\chi}\\ \|\mathbf{c}\|=1}}{\exists} : \quad \mathbf{c}^T\boldsymbol{\mathcal{W}}(t,t+\delta)\mathbf{c} < \frac{\beta^2\delta^2}{2R_m^2} := \epsilon,$$

where $\beta := \sqrt{2\epsilon}\frac{R_m}{\delta}$ and Assumption 1 was used. From this it is possible to conclude that if the conditions of the theorem do not hold, the pair $(\boldsymbol{\mathcal{A}}(t), \mathbf{C})$ is not uniformly completely observable. This pair belongs to system(7), that is related to the LTV system (5) by the Lyapunov transformation (6) that maintains observability properties. Hence, it follows that if the pair $(\mathbf{A}(t), \mathbf{C})$ is uniformly completely observable, the conditions of the theorem must hold, thus concluding the proof of the necessity part of the theorem. □

Remark 2. *The determinant in* (22) *can be written as* ${}^I\mathbf{v}^T(t_1)\mathbf{S}\left[{}^I\mathbf{v}(t_2)\right]{}^I\mathbf{v}(t_3)$. *Together with Assumption 2, this condition can be understood as a persistent excitation condition, i.e., the velocity at* t_1 *must be sufficiently out of the plane defined by the velocity at* t_2 *and* t_3 *for the vector space defined by them not to degenerate in time.*

4. Filter design and implementation

This section addresses the design of the sensor-based RO-SLAM filter. The theoretical results of the previous section were established in a deterministic setting, and thus the presence of measurement noise raises the need for a filtering solution. Theorems 2, 3, and 4 show that it is possible to design an observer with globally exponentially stable error dynamics for the nonlinear system (1). Hence, a Kalman filter follows naturally for the augmented nonlinear system (4).

Due to the discrete nature of the available sensor suite, the chosen solution is a discrete Kalman filter, and thus the continuous-time system (4) must be discretized. In this section, any quantity denoted as $(.)_k$ is the same as $(.)(t_k)$. Let T_s be the synchronized sampling period of the sensor suite and t_0 be the initial time. Then, the discrete time steps can be expressed through $t_k = kT_s + t_0$, with $k \in \mathbb{N}_O$. The process employed was the Euler forward discretization, with a small detail regarding the rotation of a landmark from one instant to the following. For the purpose of obtaining this rotation, it is considered that the angular velocity is constant over each sampling interval. It follows that

$$\mathbf{R}_{k+1}^T\mathbf{R}_k = \exp\left(-\mathbf{S}\left[\boldsymbol{\omega}_k\right]T_s\right),$$

and thus it is possible to write the discrete system dynamics

$$\begin{cases} \mathbf{x}_{k+1} = \mathbf{F}_k\mathbf{x}_k + \boldsymbol{\xi}_k \\ \mathbf{y}_{k+1} = \mathbf{H}_{k+1}\mathbf{x}_{k+1} + \boldsymbol{\theta}_{k+1} \end{cases}, \tag{29}$$

with

$$\mathbf{F}_k = \begin{bmatrix} \mathbf{F}_{L_k} & T_s\mathbf{A}_{LV} & \mathbf{0}_{n_L\times n_R} \\ \mathbf{0}_{n_V\times n_L} & \mathbf{I}_3 & \mathbf{0}_{n_L\times n_R} \\ T_s\mathbf{A}_{RL_k} & \mathbf{0}_{n_R\times n_V} & \mathbf{I}_{n_R} \end{bmatrix},$$

$\mathbf{F}_{L_k} = \text{diag}\left(\mathbf{R}_{k+1}^T\mathbf{R}_k, \ldots, \mathbf{R}_{k+1}^T\mathbf{R}_k\right)$, and $\mathbf{H}_k := \mathbf{C}_F(t_k)$. The vectors $\boldsymbol{\xi}_k$ and $\boldsymbol{\theta}_k$ represent the model disturbance and measurement noise vector, that are assumed to be zero-mean discrete white Gaussian noise. In what concerns the observability of this new discrete system, the applicability of the observability results of the previous section, derived for the continuous case, is not trivial, given the nonlinear character of the system. Nevertheless, in a previous work, the authors of [33] have designed a source-localization filter in a discrete-time setting with dynamics very similar to (29), and found observability conditions that are directly related to the ones presented here, thus hinting at the applicability of the continuous time conditions to the discrete system, and to the global exponential stability of the ensuing Kalman filter.

The signals received from the beacon landmarks are tagged, and therefore, the association of measured data with state data is trivial. For this reason, there is no need for a data association algorithm, nor for a loop closure procedure, which means that the algorithm is a standard discrete Kalman filter, (see [34]), with the detail that, when a landmark is invisible and its range is unavailable, the estimated range is used in the predict step, allowing the propagation in open loop of the invisible landmarks.

5. Simulation results

In this section, results from a typical run in a simulation setting are presented. The simulated environment consists of 20 landmarks spread randomly

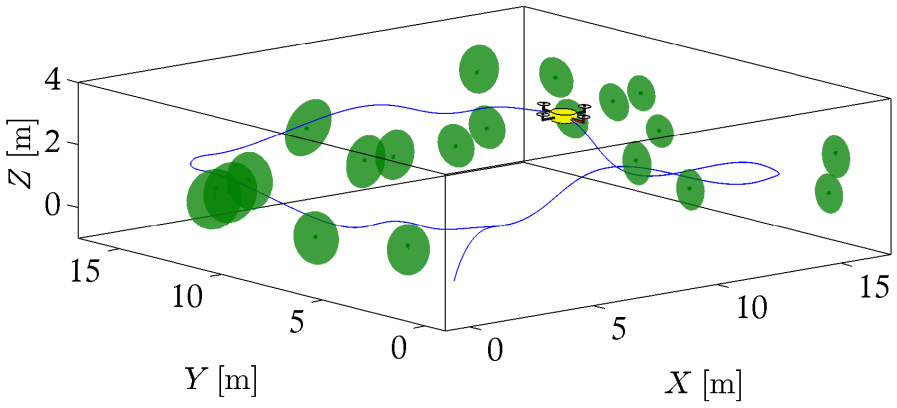

Figure 2: Picture of the estimated map rotated and translated using the true transformation at $t = 300$ s. The real trajectory is the blue line and the green ellipsoids represent the 3σ uncertainty of each landmark estimate.

Table 1: Kalman filter parameters

	Position	Velocity	Range
$\mathbf{Q}$	$T_s 10^{-3}\mathbf{I}_{3N}$	$T_s 10^{-2}\mathbf{I}_{3N}$	$T_s 10^{-5}\mathbf{I}_{3N}$
$\mathbf{R}$	–	$10^{-3}\mathbf{I}_3$	$\mathbf{I}_{N_O}$

throughout a 16m×16m×3m map. The trajectory of the vehicle was designed in order to satisfy the observability conditions, and it can be seen as the blue line in Fig. 2. All the measurements are assumed to be perturbed by zero-mean Gaussian white noise, with standard deviations of $\sigma_\omega = 0.05$ °/s for the angular rates, $\sigma_v = 0.03$ m/s for the linear velocity, and $\sigma_r = 0.03$ m for the ranges. The Kalman filter parameters were chosen as indicated in Table 1.

The performance of the RO-SLAM filter can be assessed through Fig. 3, where the norms of the estimation error of 5 landmarks are presented: after the initial transient period, the error stays within an interval with magnitude of 10 cm. The estimation error of the velocity is understandably small, as the quantity is directly observed. Its mean is below 10^{-4} m/s and its standard deviation below 10^{-3} m/s. The range error, that grows for invisible landmarks,

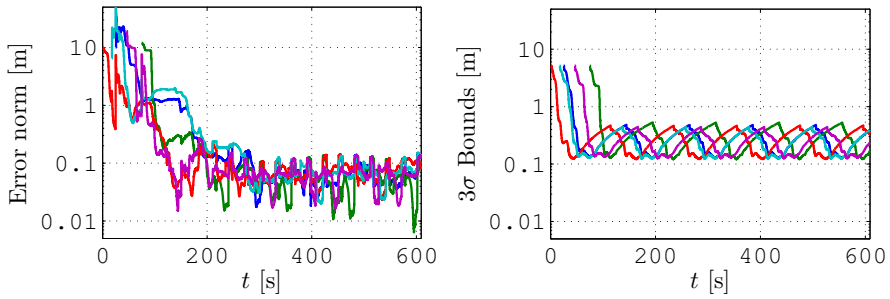

(a) Norm of the error. (b) Uncertainty.

Figure 3: Evolution of the estimation of 5 landmarks in time.

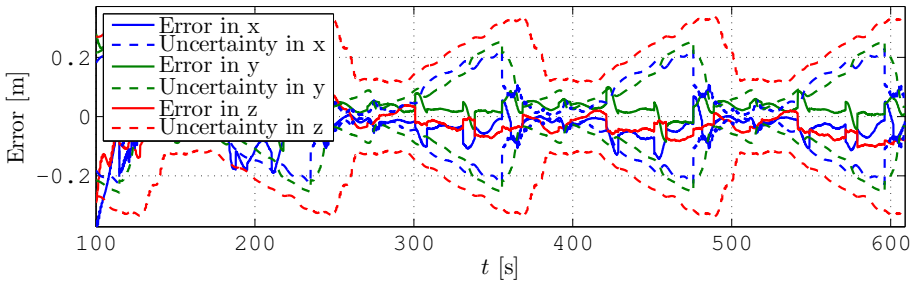

Figure 4: The estimation error of a single landmark for all coordinates with 3σ uncertainty bounds.

has a mean of 0.0266 m and its standard deviation is 0.0435 m. For better visualization, in Fig. 4 it is presented in detail the estimated errors and uncertainty bounds of a single sensor-based landmark. These results are in accordance with the theoretical results of Section 3, as the visible landmarks, as well as the other estimated quantities, converge both in uncertainty and in error. The periodic pattern that can be observed there is due to the increase and decrease of uncertainty that occurs when a landmark is not seen and suddenly reappears in the sensors field-of-view, or the persistent excitation conditions of Theorem 4 are not fulfilled.

Finally, an example of the estimated map is given in Fig. 2, where the coloured ellipsoids represent the uncertainty associated ($3\sigma_p$) and the small circles mark the true coordinates of each landmark. The yellow quadrotor marks the position of the vehicle at the time of the estimation and the blue line solid line is the real trajectory. The estimated map was rotated and translated to the inertial frame. Note that the 3σ uncertainty ellipsoids surround the true values, as they should in a consistent filter.

This simulation was designed to attest the validity of the theoretical results presented in this paper, as well as the convergence properties of the RO-SLAM filter here proposed. It was shown that the algorithm is able to produce a consistent map, depicted in Fig. 2. Moreover, the good performance of the algorithm for a sufficiently rich trajectory was demonstrated.

6. Experimental results

6.1. Setup

This section details an experiment that took place in the Sensor-based Cooperative Robotics Research Laboratory – SCORE Lab – of the Faculty of Science and Technology of the University of Macau. The experimental setup consists of an *AscTec Pelican* quadrotor instrumented with a *Microstrain 3DM-GX3-25* inertial measurement unit (IMU) working at 200 Hz, a *Microsoft Kinect*, at 10 Hz, a *Crossbow Cricket* receiver, and *VICON* markers. Furthermore, the lab was equipped with 7 more *Crossbow Cricket* motes, emitting sequentially one at a time at 10 Hz (each beacon emits every 700 ms), as well as with a *VICON* Bonita motion capture system, providing accurate estimates of the linear and angular motion quantities of the vehicle, that was used for validation of the estimates provided by the RO-SLAM algorithm.

The cricket (highlighted in red in Fig. 6(b)) is a small hardware platform consisting of a Radio Frequency (RF) transceiver, a micro-controller, and other associated hardware for generating and receiving ultrasonic signals and interfacing with a host device [27]. Each cricket beacon emits simultaneously a radio and acoustic pulse that are received by the cricket placed in the vehicle, thus allowing the computation of the ranges through difference of time of arrival of the two pulses using the speed of sound corrected by on-board temperature sensors.

The facing down camera (highlighted in blue in Fig. 6(b)) is used to compute the linear velocity of the vehicle, through the process depicted in Fig.

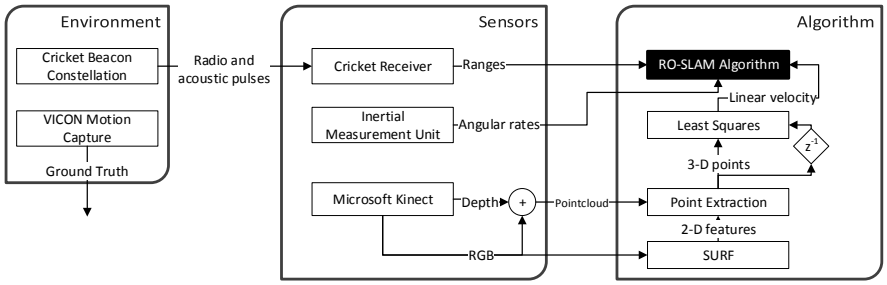

Figure 5: The flow of information in the proposed algorithm. The process employed to obtain linear velocity measurements is also explained.

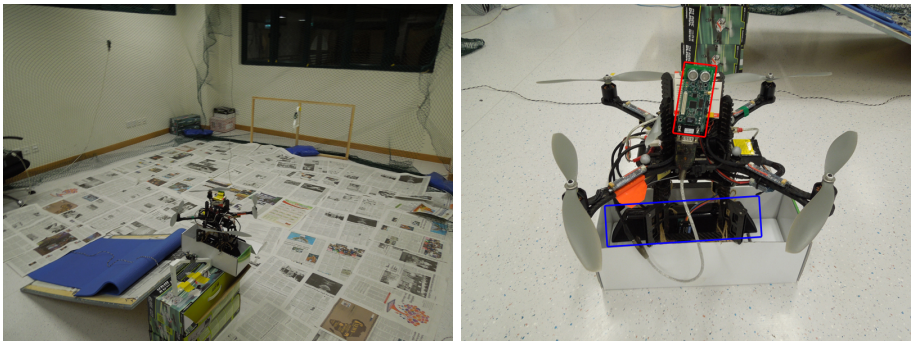

(a) The experiment area. (b) The instrumented quadrotor.

Figure 6: The experimental setup. The Cricket beacons can be seen on the left spread around the room. The Cricket receiver is mounted on the quadrotor on the right.

5. An implementation of SURF, see [35], detects features in the RGB images which correspond to tridimensional points in the Kinect pointclouds. The N_k tridimensional features ($\mathbf{f}_k^{(i)}$) of two subsequent frames are associated using a Sequential Compatibility Nearest Neighbour [11] algorithm, and then used in a Least Squares procedure to obtain the linear velocity in 3-D through the following equation

$$\mathbf{v}_k = \begin{bmatrix}\mathbf{I}_3 & \mathbf{0}_3\end{bmatrix} \left(\mathbf{H}^T\mathbf{H}\right)^{-1} \mathbf{H}^T \frac{\mathbf{f}_{k+1} - \mathbf{f}_k}{T_s}$$

where $\mathbf{H} \in \mathbb{R}^{3N_k \times 6}$ is composed of $\mathbf{H}_i = \begin{bmatrix}-\mathbf{I}_3 & \mathbf{S}\left[\mathbf{f}_k^{(i)}\right]\end{bmatrix}$. As seen in Fig. 6(a), to try to circumvent possible lack of features, the floor was covered with newspaper thus providing a good ground for feature detection.

It must be stressed that the experiments detailed in this section were designed as proof of concept, and as such, alternative sensors and processes for obtaining the linear velocity of the platform could have been employed. One possible example of alternative techniques are optical flow procedures, a com-

mon approach for velocity estimation [36].

6.2. Results

The experiment here detailed consists of series of hand-driven circular-like laps of the quadrotor in a 6m×4m area covered by the Cricket constellation (see Fig. 6). The run lasts for 5 minutes, comprising a total distance of around 90 meters at 0.270 m/s. The trajectory, shown in Fig. 9 was intended to maximize the exposure to each of the beacons, as well as to provide sufficient excitation to the filter.

Figures 7 and 8 depict the estimated position (solid blue) with 3σ uncertainty bounds of two different landmarks against the ground truth provided by *VICON* (dashed red) representing the best (landmark #1) and worst (landmark #7) estimation performance in this experiment. These quantities are accompanied by black dots indicating the observation moments, to provide better understanding of what is going on. As mentioned, each beacon emits once every 700 ms, and, due to the nature of the receiver, only one beacon pulse is received at a time. Furthermore, neither of the beacons nor receiver are omnidirectional, which means that there may occur long time intervals without any measurement from one beacon. The black dots in both Fig. 7 and Fig. 8 show the moments were each landmark is observed. As explained in Section 1, the initialization of the landmarks is one of the more challenging issues in RO-SLAM procedures. In this work, however, the global convergence results imply that this issue is solved as whichever the initial guess the filter will converge. Figures 7 and 8, where each landmark was initialized at a random point in the sphere defined by the corresponding range measurement, depict exactly this. It can be seen that the convergence is very fast in the horizontal plane, represented by Figures 7(a) and 7(b), for the first landmark, and Figures 8(a) and 8(b) for the seventh. Moreover, after converging, the estimation is very close to ground truth in the first landmark and with higher error in the seventh. However, in the vertical axis, the estimation is much worse, and the convergence is also slower, as it can be seen in Figures 7(c) and 8(c) that represent the quantities associated with the vertical coordinate. That is due to the less rich trajectory in that axis, as Fig. 9 shows. The optical flow procedure employed is somewhat noisy, and as its measurements of the linear velocity are directly used in the dynamics matrix in (29) as if they were the true value, the noise can make that direction appear observable, even if the information is sparse.

Finally, an example of the estimated map in the body-fixed frame is presented in Fig. 10. The top view of the sensor-based map is shown along with the true landmark positions and the vehicle path rotated and translated to the body-fixed frame. The coloured ellipses represent orthogonal cross-sections of 3σ uncertainty ellipsoids, i.e., the estimation uncertainty, and the small circles mark the true landmark positions.

These experiments show the good performance of the proposed algorithm in realistic conditions, especially in the horizontal variables. The filter has some problems in the vertical coordinates due to the less rich velocity profile and noisy optical flow measurements, although in Section 5 a proper trajectory

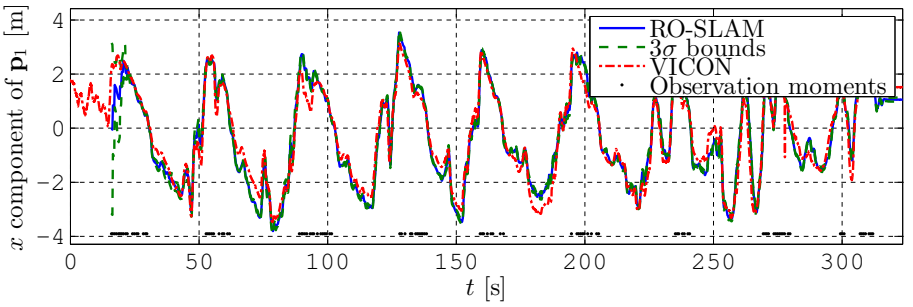

(a) x component

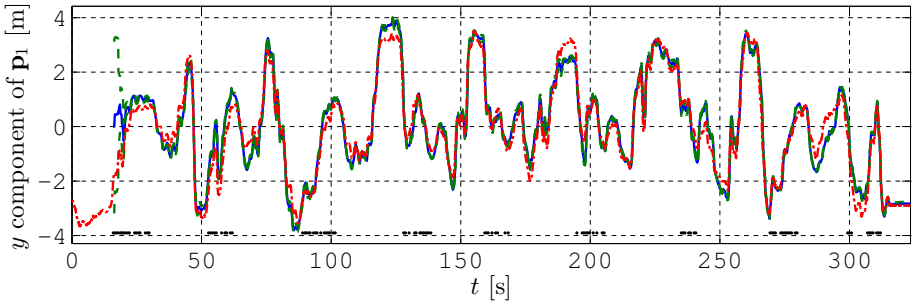

(b) y component

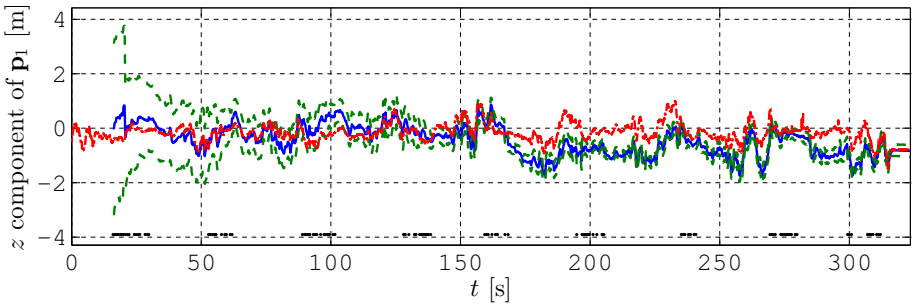

(c) z component

Figure 7: The sensor-based landmark #1 estimate against ground truth with 3σ uncertainty bounds and observation instants.

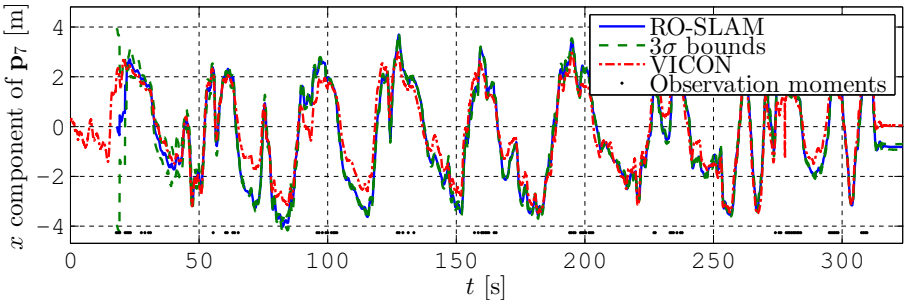

(a) x component

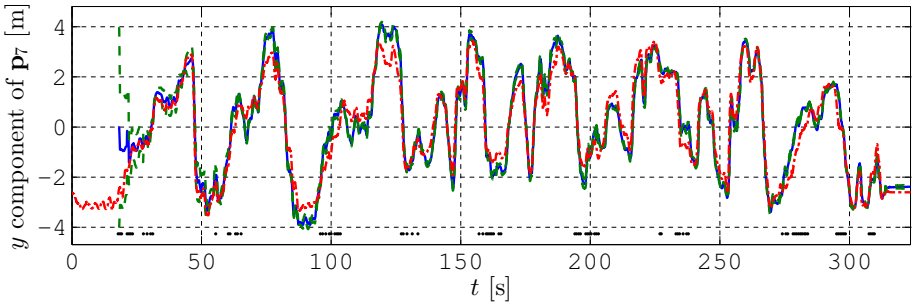

(b) y component

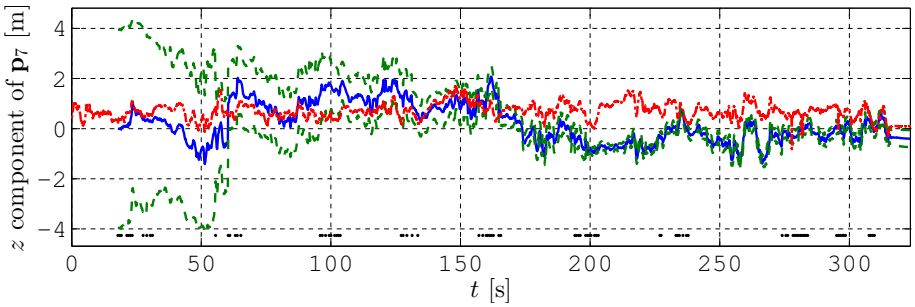

(c) z component

Figure 8: The sensor-based landmark #7 estimate against ground truth with 3σ uncertainty bounds and observation instants.

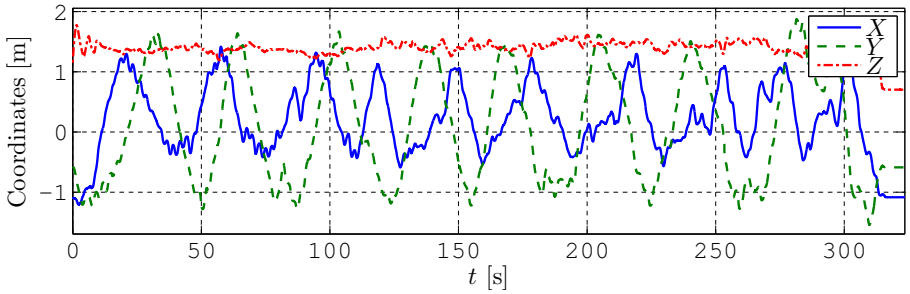

Figure 9: The position of the vehicle in time.

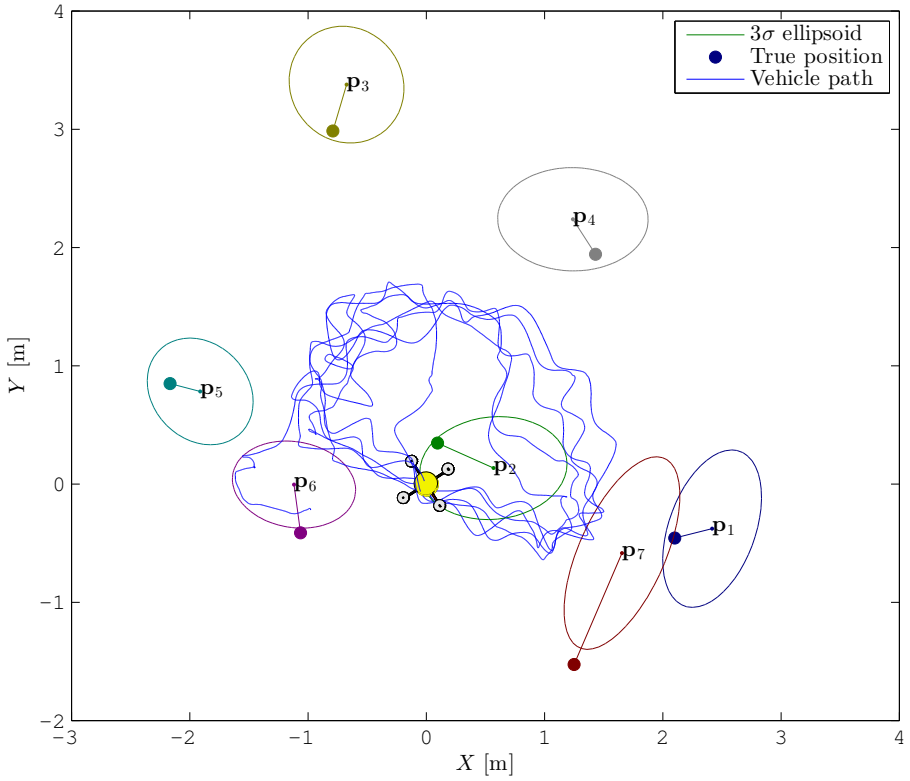

Figure 10: Top view of the estimated sensor-based map at $t = 175$ s.

was designed and the algorithm was shown to behave well. Therefore, these experiments underpin the need for appropriate trajectories.

7. Conclusions

This paper presented a novel sensor-based range-only simultaneous localization and mapping filter with globally exponentially stable error dynamics. This was achieved through state augmentation of a nonlinear system, which, along with the disposal of the non-visible landmarks, enabled regarding the resulting system as linear time-varying. The work focused on the observability analysis of the resulting system, providing theoretical observability guarantees, and equivalence between the systems used in each step of the analysis. The theoretical results include the derivation of necessary and sufficient conditions for observability, stability and convergence of the algorithm, establishing a constructive basis for trajectory design. These results were followed by the design of a Kalman filter with globally exponentially stable error dynamics. Simulations allowed the validation of the results, and real world experiments showed also the good performance of the proposed algorithm in realistic conditions while demonstrating the need for a properly designed trajectory.

Interesting points of future research are the extension of the algorithm to make use of the full capabilities of a sensor network, namely inter-sensor ranging, as well as the addition of other sensors to improve the performance, such as accelerometers.

Acknowledgments

This work was partially supported by the Fundação para a Ciência e Tecnologia (FCT) [PEst-OE/EEI/LA0009/2013]. The work of P. Lourenço was supported by the PhD Student Grant SFRH/BD/89337/2012 from FCT.

References

[1] R. Smith, P. Cheeseman, On the representation and estimation of spatial uncertainty, International Journal of Robotics Research 5 (4) (1986) 56–68. doi:10.1177/027836498600500404.

[2] R. Smith, M. Self, P. Cheeseman, Estimating uncertain spatial relationships in robotics, in: I. J. Cox, G. T. Wilfong (Eds.), Autonomous Robot Vehicles, Springer-Verlag New York, Inc., New York, NY, USA, 1990, pp. 167–193.

[3] J. Leonard, H. Durrant-Whyte, Simultaneous map building and localization for an autonomous mobile robot, in: Proc. of the IEEE/RSJ International Workshop on Intelligent Robots and Systems (IROS), Vol. 3, 1991, pp. 1442–1447. doi:10.1109/IROS.1991.174711.

[4] M. Csorba, J. K. Uhlmann, H. F. Durrant-Whyte, New approach to simultaneous localization and dynamic map building, in: Proc. of the SPIE Aerosense, Vol. 2738, 1996, pp. 26–36.

[5] S. Thrun, M. Montemerlo, The graph slam algorithm with applications to large-scale mapping of urban structures, The International Journal of Robotics Research 25 (5-6) (2006) 403–429. doi:10.1177/0278364906065387.

[6] H. Durrant-Whyte, T. Bailey, Simultaneous Localisation and Mapping (SLAM): Part I The Essential Algorithms, IEEE Robotics & Automation Magazine 13 (2) (2006) 99–110.

[7] T. Bailey, H. Durrant-Whyte, Simultaneous localization and mapping (SLAM): Part II, IEEE Robotics & Automation Magazine 13 (3) (2006) 108–117.

[8] J. Tardós, J. Neira, P. Newman, J. Leonard, Robust mapping and localization in indoor environments using SONAR data, The International Journal of Robotics Research 21 (4) (2002) 311.

[9] M. Montemerlo, S. Thrun, D. Koller, B. Wegbreit, FastSLAM: A Factored Solution to the Simultaneous Localization and Mapping Problem, in: Proc. of the AAAI National Conference on Artificial Intelligence, Edmonton, Alberta, Canada, 2002, pp. 593–598.

[10] S. Se, D. Lowe, J. Little, Mobile Robot Localization and Mapping with Uncertainty using Scale-invariant Visual Landmarks, The International Journal of Robotics Research 21 (8) (2002) 735–758.

[11] J. Neira, J. Tardós, Data Association in Stochastic Mapping Using the Joint Compatibility Test, IEEE Transactions on Robotics and Automation 17 (6) (2001) 890–897. doi:10.1109/70.976019.

[12] B. Bacca, J. Salvi, X. Cufí, Long-term mapping and localization using feature stability histograms, Robotics and Autonomous Systems 61 (12) (2013) 1539–1558.

[13] E. Jauregi, I. Irigoien, B. Sierra, E. Lazkano, C. Arenas, Loop-closing: A typicality approach, Robotics and Autonomous Systems 59 (34) (2011) 218–227. doi:10.1016/j.robot.2010.12.004.

[14] T. Bailey, J. Nieto, J. Guivant, M. Stevens, E. Nebot, Consistency of the EKF-SLAM Algorithm, in: 2006 IEEE/RSJ International Conference on Intelligent Robots and Systems, 2006, pp. 3562–3568. doi:10.1109/IROS.2006.281644.

[15] E. Olson, J. Leonard, S. Teller, Robust range-only beacon localization, IEEE Journal of Oceanic Engineering 31 (4) (2006) 949–958. doi:10.1109/JOE.2006.880386.

[16] J.-L. Blanco, J.-A. Fernandez-Madrigal, J. Gonzalez, Efficient probabilistic Range-Only SLAM, in: Proc. 2008 IEEE/RSJ International Conference on Intelligent Robots and Systems, IROS'08, 2008, pp. 1017–1022. doi:10.1109/IROS.2008.4650650.

[17] A. Ahmad, S. Huang, J. J. Wang, G. Dissanayake, A new state vector for range-only SLAM, in: Proc. of the 2011 Chinese Control and Decision Conference (CCDC), 2011, pp. 3404–3409. doi:10.1109/CCDC.2011.5968704.

[18] E. Menegatti, A. Zanella, S. Zilli, F. Zorzi, E. Pagello, Range-only SLAM with a mobile robot and a Wireless Sensor Networks, in: Proc. 2009 IEEE International Conference on Robotics and Automation, ICRA'09, 2009, pp. 8–14. doi:10.1109/ROBOT.2009.5152449.

[19] J. Djugash, S. Singh, G. A. Kantor, W. Zhang, Range-Only SLAM for Robots Operating Cooperatively with Sensor Networks, in: Proc. 2006 IEEE International Conference on Robotics and Automation, ICRA'06, 2006, pp. 2078–2084.

[20] J. Djugash, S. Singh, Motion-aided network SLAM with range, The International Journal of Robotics Research 31 (5) (2012) 604–625. doi:10.1177/0278364912441039.

[21] J. Castellanos, R. Martinez-Cantin, J. Tardós, J. Neira, Robocentric map joining: Improving the consistency of EKF-SLAM, Robotics and Autonomous Systems 55 (1) (2007) 21–29.

[22] L. Zhao, S. Huang, G. Dissanayake, Linear SLAM: A linear solution to the feature-based and pose graph SLAM based on submap joining, in: Proceedings of the 2013 IEEE/RSJ International Conference on Intelligent Robots and Systems (IROS), 2013, pp. 24–30. doi:10.1109/IROS.2013.6696327.

[23] P. Batista, C. Silvestre, P. Oliveira, Single range aided navigation and source localization: Observability and filter design, Systems & Control Letters 60 (8) (2011) 665–673. doi:10.1016/j.sysconle.2011.05.004.

[24] P. Lourenço, B. J. Guerreiro, P. Batista, P. Oliveira, C. Silvestre, 3-D Inertial Trajectory and Map Online Estimation: Building on a GAS Sensor-based SLAM filter, in: Proceedings of the 2013 European Control Conference, Zurich, Switzerland, 2013, pp. 4214–4219.

[25] P. Lourenço, B. J. Guerreiro, P. Batista, P. Oliveira, C. Silvestre, Preliminary Results on Globally Asymptotically Stable Simultaneous Localization and Mapping in 3-D, in: Proceedings of the 2013 American Control Conference, Washington D.C., USA, 2013, pp. 3093–3098.

[26] B. J. Guerreiro, P. Batista, C. Silvestre, P. Oliveira, Globally Asymptotically Stable Sensor-based Simultaneous Localization and Mapping, IEEE Transactions on Robotics 29 (6) (2013) 1380–1395. doi:10.1109/TRO.2013.2273838.

[27] N. B. Priyantha, A. Chakraborty, H. Balakrishnan, The Cricket Location-Support System, in: Proc. of the Sixth Annual ACM International Conference on Mobile Computing and Networking (MOBICOM), 2000, pp. 32–43.

[28] P. Lourenço, P. Batista, P. Oliveira, C. Silvestre, C. L. P. Chen, Sensor-based Globally Asymptotically Stable Range-Only Simultaneous Localization and Mapping, in: Proceedings of the 2013 Conference on Decision and Control, Florence, Italy, 2013, pp. 5692–5697.

[29] R. Brockett, Finite Dimensional Linear Systems, Series in decision and control, John Wiley & Sons, 1970.

[30] H. Khalil, Nonlinear Systems, 3rd Edition, Prentice Hall, 2002.

[31] B. D. O. Anderson, Stability properties of Kalman-Bucy filters, Journal of the Franklin Institute 291 (2) (1971) 137–144. doi:10.1016/0016-0032(71)90016-0.

[32] P. Batista, C. Silvestre, P. Oliveira, On the observability of linear motion quantities in navigation systems, Systems & Control Letters 60 (2) (2011) 101–110.

[33] P. Batista, C. Silvestre, P. Oliveira, GES source localization based on discrete-time position and single range measurements, in: Proceedings of the 21st Mediterranean Conference on Control Automation (MED), 2013, pp. 1248–1253.

[34] A. Gelb, Applied Optimal Estimation, MIT Press, 1974.

[35] H. Bay, A. Ess, T. Tuytelaars, L. V. Gool, Speeded-Up Robust Features (SURF), Computer Vision and Image Understanding 110 (3) (2008) 346–359, Similarity Matching in Computer Vision and Multimedia. doi:10.1016/j.cviu.2007.09.014.

[36] S. Baker, D. Scharstein, J. Lewis, S. Roth, M. Black, R. Szeliski, A database and evaluation methodology for optical flow, International Journal of Computer Vision 92 (1) (2011) 1–31. doi:10.1007/s11263-010-0390-2.